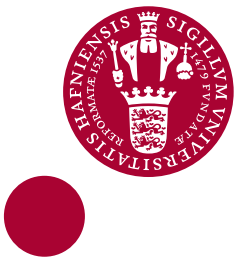

Crustal density structure of NW Iranian Plateau

Teknik, Vahid; Ghods, Alireza ; Thybo, Hans; Artemieva, Irina

Published in:
Canadian Journal of Earth Sciences

DOI:
10.1139/cjes-2018-0232

Publication date:
2019

Document version
Publisher's PDF, also known as Version of record

Crustal density structure of NW Iranian Plateau

Vahid Teknik [1,2], Abdolreza Ghods [1], Hans Thybo [3,4], Irina M. Artemieva [2]

(1) Institute for Advanced Studies in Basic Sciences, Department of Earth Sciences, Zanjan, Iran.
(2) University of Copenhagen, Department of Geosciences and Natural Resource Management, Copenhagen, Denmark.
(3) Eurasia Institute of Earth Sciences, Istanbul Technical University, Istanbul, Turkey.
(4) University of Oslo, Centre for Earth Evolution and Dynamics, Oslo, Norway.

Abstract

We present a new 2D crustal-scale model of the NW Iranian plateau based on gravity-magnetic modeling along the 500 km long CIGSIP seismic profile across major tectonic provinces of Iran from the Arabian plate into the South Caspian Basin (SCB). The seismic P-wave receiver function model along the profile is used to constrain major crustal boundaries in the density model. Our 2D crustal model shows significant variation in the sedimentary thickness, Moho depth and the depth and extent of intra-crustal interfaces. The Main Recent Fault between the Arabian crust and the overriding Central Iran crust dips at ~13° towards the NE to a depth of ~40 km. The geometry of the MRF suggests ~150 km of underthrusting of the Arabian plate beneath Central Iran. Our results indicate the presence of a high-density lower-crustal layer beneath Zagros. We identify a new crustal-scale suture beneath the Tarom valley between the South Caspian Basin curst and Central Iran and the Alborz. This suture is associated with sharp variation in Moho depth, topography and magnetic anomalies and is underlain by a 20 km thick high-density crustal root at 35-55 km depth. The high density lower crust in Alborz and Zagros may be related to partial eclogitization of crustal roots below ~40 km depth. The gravity and magnetic models indicate a highly extended continental crust for the SCB crust along the profile. Low observed magnetic susceptibility at the Kermanshah ophiolites probably implies that the ophiolite rocks only form a thin layer which has been thrust over the sedimentary cover.

Keywords: 2D forward crustal modeling, Gravity and Magnetic anomalies, Receiver function, Iranian plateau, Moho, Sediment thickness.

1. Introduction

The Iranian Plateau formed by long-lasting convergence and collision between the Arabian and the Eurasian plates. The interaction between these two major lithospheric plates and numerous microplates trapped between them created a broad zone of deformation with different type of structural units, similar to the tectonic style named Turkic-type (Şengör and Natalin, 1996). Tectonically, the region is divided into several major units, namely the Zagros fold and thrust belt, the metamorphic Sanandaj-Sirjan Zone (SSZ), the Tertiary Urmia-Dokhtar Magmatic Arc (UDMA), the Central Iran Zone, Alborz and the South Caspian Basin. **Figure 1** shows a proposed schematic cross section across the deformation zone, constructed based on commonly accepted views (e.g. Berberian and Berberian, 1981; Stocklin, 1968). The deformation style in this region is highly influenced by the evolution of the Tethyan oceans and collision of Arabian and Central Iran plates as evidenced by Tertiary magmatism associated with paleo-subductions and the presence of ophiolites, respectively. The different geotectonic units were mainly studied and categorized by numerous surface and near-surface geological surveys but the relationships between the units and deep crustal structures are not yet clear.

The geometry and density of intra-crustal layers of the Iranian crust are poorly studied and most of the seismic crustal studies focus on estimation of the Moho depth (e.g., Hatzfeld et al., 2003; Paul et al., 2010; Tatar and Nasrabadi, 2013). The thickness of the sedimentary cover is an important geophysical parameter. Previous geophysical interpretations of the lithosphere structure in Iran (Jimenez-Munt et al., 2012; Motavalli Anbaran et al., 2011; Tunini et al., 2015) have been carried out without exact knowledge of the geometry and composition of intra-crustal layers including the thickness of the sedimentary cover. These interpretations are along linear profiles

and are mainly based on integrated geophysical modeling of gravity, geoid, and topography together with the sparsely distributed observations of surface heat flow. These profiles are unconstrained by independent seismic observations from receiver function or active seismic sections. In the mentioned models, much of the observed gravity signal is related to the shape of lithospheric-asthenospheric boundary and, in some cases (Tunini et al., 2015), to assumed petrological heterogeneity in the mantle lithosphere.

In this paper, we present a new high resolution crustal model of the NW Iranian plateau along a profile coincident with the CIGSIP (China-Iran Geological and Geophysical Survey in the Iranian plateau) seismic profile. The profile crosses all major tectonic units of the NW Iranian plateau (**Figure 1**) providing an excellent opportunity to investigate the crustal structure of the tectonic units and their relations. The 2D model includes sedimentary cover, and crustal interfaces and Moho as constrained mainly by a receiver function seismic section (Chen et al., 2016). We model the density and susceptibility distribution between the boundaries in order to improve our understanding of deep crustal processes. In our adopted top-down modeling strategy, we calculate the effect of crustal structure on the observed gravity signal and relate the residual to structure in the upper mantle.

Based on the modelled geometry, density and susceptibility of the crust, we discuss the following questions: (1) How has the convergence between the Arabian and Eurasian plates been accommodated in the crustal layers and how much shortening is accommodated in the lower crust? (2) Has crustal thickening been accompanied by eclogitization of the lower crust beneath the deep mountain roots? (3) What is the nature of the crust below the South Caspian Basin (i.e., oceanic or continental)?, and (4) How thick are the exposed ophiolites along the suture between Arabian and

86 Central Iran plates ?

87 ## 2. Geological Setting

88 The study region includes two orogenic systems, which developed in response to collision
89 between the Arabian plate and the Eurasian plate. The Zagros-Makran orogenic system in the
90 southern part of the Iranian plateau formed along the NE margin of the Arabian plate, whereas the
91 Talesh-Alborz-Kopeh Dagh mountains in the north of the plateau follow the boundary between the
92 Central Iran Zone and the south Caspian basin of the Eurasia plate (e.g., Hatzfeld and Molnar,
93 2010).

94 The Zagros mountains preserve a record of the long-lasting convergence across the Neotethys
95 from subduction to the present-day collision (~90 Ma to present, Agard et al., 2011). The Main
96 Recent Fault (MRF) represents a Neotethian suture zone in the Zagros orogeny (Agard et al.,
97 2011). The Zagros orogenic system from NE to SW includes three major parallel tectonic zones:
98 the Urmia-Dokhtar Magmatic Arc, the Sanandaj-Sirjan metamorphic-magmatic zone, and the
99 Zagros fold and thrust belt. (**Figure 2a**) (e.g., Manuel Berberian and King, 1981; Stocklin, 1968).

100 The Sanandaj-Sirjan metamorphic and igneous zone is a ribbon-like northwest trending belt,
101 located immediately to the north of the Zagros suture (Stocklin, 1968) with a basement consisting
102 of metamorphic, igneous and sedimentary rocks (e.g., Richards and Şengör, 2017). The initial
103 subduction of the oceanic slab of Neotethys beneath Central Iran formed the Andean type
104 Sanandaj-Sirjan zone. After a possible first slab break-off at ~60-55 Ma, the subduction of the
105 Neotethys oceanic slab continued at a lower angle and formed the Andean type Urmia-Dokhtar
106 magmatic arc to the north of the Sanandaj-Sirjan Zone. The low angle subduction and its

107 associated volcanism was mainly active up to Oligo-miocene time (~35-25 Ma), the approximate
108 collision time of the Arabian plate with Central Iran (e.g., Agard et al., 2011).

109 The Zagros fold and thrust belt is generally regarded as one of the youngest collisional belts on
110 Earth, hosting considerable oil and gas resources. There is general agreement that deformation is
111 mainly accommodated by folding in the sediments and thrust faulting in the crystalline basement
112 and sedimentary cover, with a high level of seismicity (e.g., McQuarrie, 2004; Tatar et al., 2004).
113 The Zagros fold and thrust belt is separated from the Mesopotamian foreland basin by a main
114 structural uplift of several kilometers along the Main Frontal Fault (MFF). Our profile crosses the
115 NW part of Zagros named the Lurestan arc (**Figure 1a**). It is located to the north of the high
116 resolution receiver function Zagros 2003 profile (Motaghi et al., 2017), which detected the
117 presence of a low angle seismic interface to a depth of about 17 km within the Lurestan arc.
118 Motaghi et al., (2017) speculate that seismic deformation in the Lurestan arc is mzinly
119 accommodated by low angle thrust faulting along this intra-crustal seismic interface.

120 The collision of the Cimmerian continental fragment with the Eurasian plate in the Late Triassic to
121 Early Jurassic formed the Talesh-Alborz mountain ranges along the paleo-Tethys suture zone
122 (**Figure 1a**). The Alborz mountain range is situated between the South Caspian Basin (SCB) and
123 the central Iranian block. The Alborz orogenic belt is narrow (120–150 km wide) and it is
124 commonly accepted that the orogeny is bounded by south and north-dipping thrust faults at its
125 northern and southern flanks (e.g, Allen et al., 2003; Guest et al., 2007; Şengör et al., 1984).

126 It is difficult to assess the active faulting along the northern margin of the Alborz Mountains due
127 to the poor basement exposure. The so-called Khazar fault is generally interpreted as a transition
128 zone between the Central Iran plate and the SCB. Tatar et al. (2007) interpret south dipping thrust

129 faulting on the Khazar fault and underthrusting of the South Caspian basin beneath the Alborz
130 Mountains during the 2004 Baladeh 6.2 Mw earthquake (Tatar et al., 2007). However, four
131 seismic receiver function sections and the seismicity pattern along the Caspian Sea have not
132 identified evidence for underthrusting of the SCB beneath central Iran along the Khazar fault
133 (Ghods et al., 2016).

134 Within the study area, the major zones of seismicity are in Zagros and Alborz. The deformation
135 of the upper crust in the study area has resulted in thrust and strike-slip faulting (Talebian and
136 Jackson, 2002) (Figure 1). The most aseismic blocks are the Sanandaj-Sirjan Zone and the interior
137 of SCB. Seismicity in northern Iran is limited mainly to a belt along the Alborz mountain belt,
138 where seismic activity occurs primarily in the upper crust at depths shallower than 15 km depth.
139 The South Caspian basin has almost no seismicity and is considered as a rigid block (e.g., Engdahl
140 et al., 2006; Jackson et al., 2002)(**Figure 1a**). Relocation of seismicity in the western part of SCB
141 does not support underthrusting of the SCB beneath the Talesh mountains (Aziz Zanjani et al.,
142 2013).

143 The Central Iran tectonic block is located at a roughly triangular area in the middle of the Iranian
144 plateau, bordered by the Alborz mountains in the north and the Sanandaj–Sirjan zone in the south-
145 southwest (e.g, Stocklin, 1968). It includes orogenic belts, metamorphic zones, magmatic arcs and
146 sedimentary basins. The block separated from Gondwana in the Late Paleozoic and was accreted
147 to Eurasia in the Mesozoic during the Cimmerian collisional events (e.g., Guest et al., 2007;
148 Zanchi et al., 2009). Aseismic zones surrounded by seismic zones are characteristic of this region
149 (Engdahl et al., 2006).

150 The origin of the South Caspian Basin is controversial and it is interpreted as a remnant of

Paleotethyan oceanic crust, a trapped remnant of early Mesozoic oceanic crust, a Cretaceous to Paleogene strike-slip-related continental pull-apart basin, or a Middle to Late Jurassic marginal basin of the Tethys ocean (Guest et al., 2007 and references therein). Seismic studies suggest a more than 15-25 km thick sedimentary cover above a 15-18 km thick mafic crystalline basement (e.g., Brunet et al, 2003).

3. Datasets

Our density and susceptibility model is based on geological and tectonic mapping, depth to magnetic basement and a P-wave receiver function model of the main crustal interfaces. The available geological and geophysical data are used in the modeling process to construct the geometry of the initial model, including thickness of the sedimentary cover, the depth to intra-crustal interfaces and the Moho.

P-wave receiver function model: The depth to the Moho is constrained by the seismic receiver function profile (Chen et al., 2016) along our profile. The broadband temporary CIGSIP seismic project deployed 63 stations, which operated from October 2013 to October 2014. The NE-SW trending seismic array includes three linear parallel seismic lines from the south of the Zagros Fold and Thrust Belt to the coast of South Caspian Sea. The main line of the array is ~550-km long and includes 46 stations with a station spacing of 10-15 km.

Teleseismic data recorded by the CIGSIP temporary linear array image the subsurface velocity interfaces. P receiver functions were calculated by analysis of teleseismic events recorded within epicentral distance of 25°-95° and magnitude ≥ 5.5. The ZNE waveforms were windowed from 50 s before and 100 s after the onset of direct P phase and rotated into the ZRT coordinate system. A

time domain maximum entropy deconvolution method (Wu and Zeng, 1998) was used to eliminate the source effects and isolate P to S conversions on the R component. A Gaussian parameter of 5 and a water level of 0.0001 were adopted in the deconvolution. The resultant receiver functions were further bandpass filtered with corner frequencies of 0.03 Hz and 1 Hz to remove the high-frequency noise.

Along the profile, the tectonic units are bounded by major thrust and strike-slip faults. The Main Recent Fault (MRF) is the suture zone between the Arabian plate and the central Iranian micro-plates (Berberian, 1995). Figure 3 shows all positive and negative convertor interfaces extracted from the RF profile (Chen et al., 2016). The RF profile shows a strong northward dipping negative impedance interface at a distance range of 150 - 300 km which continues from the surface trace of the MRF to a depth of ~40 km, implying about 150 km of underthrusting of the Arabian crust beneath Central Iran. We interpret the low velocity associated with the negative impedance contrast as evidence for a shear zone of the MRF. The dipping interface is similar to the MRF fault zone interpreted by Paul et al., (2010) along the Zagros 2003 seismic profile in the southern part of the Lurestan arc and suggests underthrusting of the Arabian plate under the southwestern edge of the Iranian Plateau. Similar negative conversion interface has been also observed in Himalaya (Nábělek et al., 2009).

Two positive impedance interfaces are observed in the shallow crust of the Zagros belt. The first near-surface seismic interface (8 to 10 km) is nearly flat beneath the entire Lurestan arc (**Figure 3**). This boundary is interpreted as the base of the sedimentary cover, in agreement with geological studies (Malekzade et al., 2016; Vergés et al., 2011b). Another flat intra-crustal seismic interface is observed at ~17 km depth to the south of the suture zone (~150 km profile distance). A similar

194 feature has been reported along another profile (i.e., Zagros 2003 profile (Paul et al., 2010) to the
195 south of Lurestan arc (Motaghi et al., 2017) as a significant crustal interface between the upper and
196 middle crust. The recent 7.3 Mw Sarpolzahab (**Figure 1a**) low angle thrust earthquake (12
197 November 2017) was located at the same depth as this interface.

198 The RF section (**Figure 3**) shows a gradual crustal thickening from ~50 km in the southern end of
199 the profile to its maximum thickness beneath the MRF (~65 km), which demonstrates substantial
200 crustal thickening in the Zagros orogen. From the SSZ to the Alborz Mountains, the Moho depth
201 decreases gradually from ~55 km to ~45 km. In the middle of the Alborz Mountains or more
202 precisely at the northern boundary of the Tarom valley, the Moho boundary steps from ~45 km to
203 ~30 km (Chen et al., 2016) or to 40-55 km as indicated in our study. The sudden jump of the
204 Moho around a distance of 500 km may be related to the boundary between SCB and the Central
205 Alborz crust (Ghods et al., 2016). The RF section shows a deeper, weak, positive impedance
206 boundary beneath the Tarom valley.

207 **Sediment thickness:** A significant part of the Iranian plateau is covered by a thick sedimentary
208 cover in the Zagros, Kopeh Dagh and Makran (Teknik and Ghods, 2017). Aeromagnetic data can
209 provide a proxy for the thickness of sedimentary cover by estimates of the depth to the magnetic
210 basement based on the radially averaged power spectrum method (e.g. Maus and Dimri, 1995).
211 This approach assumes that the sedimentary cover is much less magnetized than the crystalline
212 basement (**Figure 2b**) (Teknik and Ghods, 2017).

213 The thickness of the sedimentary cover can also be estimated by the RF method. The basement is
214 expectedly the shallowest strong, positive impedance interface in the seismic receiver function
215 section, because sediments have lower seismic velocity than the basement. In our approach we

constrain the thickness of the sedimentary cover as the depth to the shallowest seismic interface in the RF model (Chen et al., 2016; Paul et al., 2010), the depth to magnetic basement (Teknik and Ghods, 2017), and the thickness of the stratigraphic column as derived from basin analysis studies (**Figure 2b**) (e.g., Vergés et al., 2011a).

3.3. Gravity data: We use Bouguer anomaly data over the study area as retrieved from the world database of BGI (Bureau Gravimétrique International), which has sparse coverage in Iran. The data coverage is sufficiently dense for regional-scale tectonic studies. The main feature of the gravity field is a wide, long wavelength negative Bouguer anomaly (minimum of -150 mGal) trending parallel to MRF with a NW–SE trend and centered roughly 150 km NE of the MRF. At the northern margin of the Central Iranian block, the gravity field increases smoothly reaching up to 50 mGal on the northern side of the Alborz Mountains (**Figure 2c**).

3.4. Aeromagnetic data: To identify the major tectonic units of Iran, an aeromagnetic survey was conducted by Aeroservice (Houston, Texas) during 1974-1977 under the auspices of the Iranian Geological Survey. We use the composite aeromagnetic 1 km × 1 km grid calculated from the original raw data (Saleh, 2006). The data are reduced to the pole using the variable RTP method (Paterson Grant & Watson Limited (PGW), 1973) (**Figure 2d**).

Along our profile, the aeromagnetic anomaly shows insignificant variation over the Zagros fold and thrust belt and sharp variation above the MRF fault zone, which probably is caused by strongly magnetized ophiolites near the suture zone and/or surface displacement associated with MRF. The pattern of magnetic anomalies in the SSZ unit may be caused by a relatively deep-seated igneous intrusion. It is widely accepted that igneous rocks are present as intrusions in the sedimentary rocks in the SSZ and Central Iran block (e.g., Verdel et al., 2011). Near Qorveh city,

an anomaly named here as the Qorveh anomaly (QA) indicates the presence of a possible intrusion of igneous rocks into or below the sedimentary cover. We consider this anomaly to be caused by a single intrusion in our susceptibility model. Magnetic anomalies show strong variation in the middle of the Alborz Mountains, which we interpret as the border between the Central Iran and the South Caspian block (**Figure 4**).

Depth variations in the Curie isotherm are usually identified by long wavelength magnetic anomalies because of a deep source. Long wavelengths (greater than 150 km) magnetic anomalies reveal two consecutive pairs of positive-negative anomalies, which may reflect Curie isotherm depth variations, lateral crustal susceptibility variations, or a combination of both. The Tertiary magmatic arc near the Alborz Mountains is associated with a broad positive magnetic anomaly, which suggests a combined effect of near-surface high susceptibility magmatic rocks and the Curie depth variations at depth. The origin of some of the observed anomalies may have alternative explanations. For instance, positive magnetic anomalies PM1 and PM2 can be associated with either a slightly deep Curie isotherm or the presence of a wide body of high susceptibility material at shallow depth. The NM1 and NM2 negative magnetic anomalies can also be explained by the presence of a thin magmatic body or by a shallow wide susceptibility rock body in the crust (**Figure 4**).

4. Modeling

We apply constrained forward modeling of the crustal density and susceptibility distribution along a profile in NW Iran. The two dimensional (2-D) model is constrained by the geometry of crustal layers derived from the seismic receiver function study (Chen et al., 2016) along the profile. The

best fitting model is determined by iterative fine-tuning of parameters within the frame of all available geological and geophysical constraints until the model response optimally fits the observed gravity and magnetic anomalies. In Appendix A, we present complementary tests to assess the uniqueness of the model.

Density Modeling: The 2D forward density model was constructed by using additional constraints in a stepwise manner to reduce the uncertainty of the model, and to assess the effect of each model parameter on the misfit. The first step includes determination of the geometry of the expectedly strongest density contrasts at the base of the sedimentary succession and at the base of the crust. The basement depth is determined as described above. The geometry of the Moho is initially constrained by the receiver function profile and was later fine-tuned by the long wavelength Bouguer gravity signal in order to reduce uncertainties caused by depth conversion and migration of the RF section. These uncertainties originate primarily from the velocity model that is based on surface wave noise tomography (Jiang et al., 2016).

For the density of crustal units, we used a range of density values as obtained from global crustal velocity studies and the Nafe-Drake relationship between velocity and density. Global and regional crustal studies (e.g. Artemieva and Thybo, 2013; Rudnick and Fountain, 1995) indicate that continental crust is highly heterogeneous in three dimensions. However, it is useful to divide the crust into the sedimentary cover and upper, middle, and lower crystalline crust (e.g. Lyngsie et al., 2006; Thybo, 2001). These layers have distinctively different densities. Average density, ρ, of sedimentary cover, upper crust, middle crust and lower crust are $\rho < 2650$ kg/m^3, $\rho < 2800$ kg/m^3, $2800 < \rho < 2900$ kg/m^3, and $2900 < \rho < 3000$ kg/m^3, respectively. Average density of high-velocity lower crustal layers observed in some tectonic regions is $\rho > 3000$ kg/m^3. Average density of the

upper mantle is larger than 3200 kg/m^3 (Artemieva and Thybo, 2013).

To construct our density model, we fixed the Moho interface at the base of the model and thickness of sedimentary cover at the top. On this basis, the crust is divided into smaller blocks based on intra-crustal boundaries observed in the seismic model. Finally, the density of each block is adjusted to improve the fit. In our final model, we do allow for reduction of density with depth if it is required by the RF section. The density modeling includes the following steps:

Step 1: Density is calculated for a simple model with three layers representing the sedimentary cover, crystalline crust, and upper mantle. The base of the sedimentary cover is defined as the shallowest positive interface in the RF section (Chen et al., 2016) (**Figure 3**). The depth of magnetic basement (Teknik and Ghods, 2017) is in overall agreement with the depth of sedimentary cover extracted from the RF section, although it is shallower over the Kermanshah ophiolite outcrops and considerably deeper in the western part of the Lurestan arc.

The initial density model has a homogeneous sedimentary cover, crystalline crust, and upper mantle with assumed densities of 2450, 2820 and 3270 kg/m^3, respectively. The shape of the calculated gravity Bouguer anomalies is similar to the observed data but with a large misfit. The root mean square (RMS) difference between the observed data and the calculated response is ~85 mGal. The calculated gravity response of the model has a broad and strong negative gravity anomaly in the Zagros, the SSZ, and Central Iran, while in the northern part of the profile the calculated gravity is considerably larger than observed.

Step 2 (**Figure 5**)*:* The RF model includes two flat and positive converters below the sedimentary cover beneath the Zagros part of the profile at depths of 8-10 km and 16-18 km. The seismic interface at 8-10 km depth is considered as the base of the metamorphosed sedimentary cover. In

this step, we assume that the seismic interface at ~17 km depth separates the upper and middle crust. The upper and middle crust are assigned density values of 2750 and 2800 kg/m^3. The positive converter in the RF model at depth ~35 km (profile distance 100 -250 km) is assumed to separate the middle and the lower crust. Assigning a density value of 3050 kg/m^3 to the lower crust of the Zagros fold and thrust belt (ZFTB) decreases the misfit between the computed and the observed gravity.

The RF model suggests two possible depths for the Moho boundary around the Tarom valley. The depth of the shallower, high-amplitude boundary interface (shown by number 1 in **Figure 5**) decreases sharply from 50 km to 30 km under the Tarom valley. The second, less distinct, converter (shown by number 2 in **Figure 5**) represents an alternative converter for the Moho. We find that assigning a high crustal density of 3100 kg/m^3 to the lower crust between converters 1 and 2 in this region decreases the calculated anomaly to the level of the observations and, therefore, reduces the misfit significantly. Thus, we consider the deeper boundary as the Moho. The structural differences associated with the sharp variations in the topography and aeromagnetic anomaly (**Figure 4**) suggests the presence of a transition zone between Central Iran and South Caspian Basin around the Tarom valley.

The RMS misfit between the calculated and the observed gravity anomaly is reduced to around 24 mGal. In the central part of the profile, the calculated response is less than the observation and thus requires a denser lower crust in parts of Zagros, Central Iran and SCB.

Step3 (**Figure 6**)*:* In this stage, we consider the compaction of the sedimentary cover with depth. Sedimentary layers deeper than 5 km depth are expected to be highly compacted, leading to a low density contrast at the sedimentary-crystalline rocks interface (e.g. Chakravarthi, 1995; Rao,

1986). Therefore, we assign a density of 2400 kg/m^3 to sediments shallower than 5 km and 2550 kg/m^3 to sediments deeper than 5 km. We also introduce a high density (2950 kg/m3) lower crustal layer for Central Iran and SCB.

We speculate that the underthrusting of Zagros lithosphere beneath the Iranian crust has produced downward bending of the upper crust of Zagros to the extent that it is juxtaposed below the middle crust of the Iranian crust. This scenario would explain the observed strong, dipping, negative converter related to MRF (**Figure 3**). In this stage of modeling, we further modify our model to consider the downward bending of the Zagros upper crust (**Figure 6**). We also model a possible low velocity (and density) zone in a more straight way by introducing a low density area (**supplementary material, Figure A7)**, but because the width of the low velocity zone is small (about 7 km), the gravity anomalies are not sensitive to the presence of the low density area.

Beneath the Tarom valley, the negative localized converter at around 500 km together with the steep local gravity high indicate the presence of a shallow high density body, which may have its origin as a magmatic intrusion or an ophiolite that is today hidden beneath the sedimentary cover. The density of the shallow high density Caspian block is estimated to be 2950 kg/m^{3,} which is higher than normal upper crustal values. The Bouguer gravity map (**Figure 2c)** shows a high amplitude short wavelength Bouguer anomaly along the south and southwest borders of Caspian Sea. We speculate that this unusually dense body in the upper crust may be related to mafic rocks associated with an ancient rift system. The three mentioned modifications of the model have reduced the RMS misfit to ~6.5 mGal.

In the above three steps, we did not include any lateral or depth variation of density in the upper mantle and instead assigned an average density of 3270 kg/m^3 to the upper mantle. Our density

model has a very low RMS misfit which suggests that most of the Bouguer gravity signal may be related to crustal anomalies. Joint teleseismic-regional travel time tomography of lithospheric structure in NW Iran indicates that the pattern and amplitude of crustal Pn residuals are very similar to those obtained from teleseismic P travel times ((Alinaghi et al., 2007; Bavali et al., 2016; Rahmani et al., 2018). This implies that crustal heterogeneities are responsible for a significant part of the teleseismic P travel time residuals, thus supporting our modelling result.

Magnetic Susceptibility modeling: On crustal scale, the magnetic crust can be simplified into three main layers based on the generally accepted range of susceptibility values: 1) near-surface magmatic intrusions and ophiolites, 2) the sedimentary layer with insignificant susceptibility, and 3) the magnetic crust from the bottom of the sedimentary cover to the Curie Depth Point (CDP) with an average susceptibility of 0.035 SI (e.g., Clark and Emerson, 1991; Hunt et al., 1995). CDP is the depth at which magnetite, the dominant magnetic mineral in the deep crust, loses its magnetization at ~580°C. We apply forward modeling to estimate CDP instead of the widely used spectral methods (e.g. Bouligand et al., 2009; Maus and Dimri, 1995), which may lead to serious errors (Teknik and Ghods, 2017). The susceptibility of the sedimentary strata is not sensitive to compaction and thus the susceptibility contrast at the interface between sediment and crystalline rocks is not sensitive to the depth of the interface. The insignificant susceptibility of the sedimentary cover allows use of magnetic data to map the magnetic basement topography.

At the first step of forward magnetic modeling, we fix the thickness of sedimentary cover based on the results of the density modeling. A constant low susceptibility value of 0.01 SI is assigned to the sedimentary cover. We also assume a constant CDP at 40 km depth to detect the presence of significant near surface intrusions and ophiolites (**Figure 7**). The CDP depth only affects the long

wavelengths of the observed magnetic anomalies whereas the shallow magnetized sources mostly control the short to medium wavelengths of the magnetic anomalies.

The high amplitude magnetic anomaly in the southern hills of Alborz (labeled as TMA in **Figure 4** and **7**) corresponds to the Tertiary (i.e., Eocene) Alborz magmatic arc belt. The shape of the magnetic anomaly correlates with the ~150 km wide surface outcrop of volcanic rocks (**Figure 2a**) as mapped in 1:100 000 scale geological maps of the Geological Survey of Iran (Nogole-Sadat, M.A.A. and Almasian, 1993). A susceptibility value of 0.175 SI is assigned to this near surface volcanic unit. The next short wavelength magnetic anomaly is within the Bijar sedimentary basin in the SSZ (Teknik and Ghods, 2017) and suggests the presence of a hidden magnetized intrusion at the Qorveh anomaly, beneath the sedimentary cover (**Figure 2d** and **7**). We assign a susceptibility value of 0.095 SI to this intrusion. A smaller amplitude magnetic anomaly near the MRF (**Figure 4** and **7**) corresponds to the Kermanshah ophiolites, which we assign a susceptibility of 0.065.

The three anomalous bodies corresponding to the Kermanshah ophiolite, Qorveh intrusion, and the Tertiary magmatic arc of Alborz (**Figure 7**) provide a close match to the general magnetic profile, although some long wavelength misfit between the observed and the calculated anomaly remains (highlighted with a thick gray line in **Figure 7**) with peak values between ~-100 and 150 nT. The long wavelength of the residuals implies a deep source such as variations in the depth to the CDP isotherm. The negative correlation between the residual curve and the long wavelength part of magnetic anomalies (compare **Figure 4** with **Figure 7**) suggests that the residuals represent variation in the depth to the Curie temperature, although there may be other sources involved. Because of the uncertainties, we do not interpret the variations of CDP in full detail, and instead

we mainly model the lateral variation of the total susceptibility of the crystalline crust. The final magnetic model shows a close correlation between the data and the calculated anomalies.

Modeling uncertainties and non-uniqueness of the results: The gravity and magnetic responses of the model are sensitive to the geometry of the intra-crustal interfaces used in the model. A combination of different density and magnetic susceptibility with different geometries of intra-crustal interfaces can produce similar gravity or magnetic responses. Uncertainties in the geometry and densities of intra-crustal layers generally increase with depth. We have reduced the geometry-related uncertainties by using independent constraints on the geometry from a seismic receiver function model and the observed near surface structures, including distribution of magmatic intrusions, suture zones and thickness of sedimentary cover. Probably the most important uncertainty of the 2D model is the presence of large 3D lateral and depth density and susceptibility variations. However, our profile is perpendicular to the major tectonics trend, which reduces this uncertainty, and we assume insignificant density and susceptibility variations normal to the profile direction. In Appendix A, we present complementary tests to assess further the uniqueness of the model presented in **Figure 6**. We test the sensitivity of the density model in relation to key parameters, including the Caspian dense shallow body, the upper, middle and lower crust, Zagros root and Alborz root. The sensitivity analyses were undertaken to understand how density variations within plausible ranges may affect the response of the density model. The tests prove that the model presented in **Figure 6** is the most reliable density model.

5. Results and discussions.

We present a 2D-crustal density and magnetic susceptibility model in NW Iran. The model

includes thickness of sedimentary cover, depth to intra-crustal interfaces and the Moho, Curie depth point, and variation in crustal density and magnetic susceptibility.

Sediment thickness: The depth to magnetic basement is in overall agreement with the thickness of the sedimentary cover interpreted from the RF section (**Figure 3**). Our results indicate that the thickness of sediments in the ZFTB is ~8 km. This value is in agreement with estimates from structural geological studies (e.g., Vergés et al., 2011a, 2003), but in sharp disagreement with the depth to magnetic basement calculated by the fractal spectral analysis method (Teknik and Ghods, 2017)(**Figure 2b**). We speculate that the ~17 km depth to magnetic basement in the Lurestan arc (distances 0-30 km in **Figure 2b** and **Figure 3**) is related to possible intense upper crust deformation associated with the low angle thrusting in the region (Motaghi et al., 2017) which may have destroyed the magnetization of the upper crustal layer.

Ophiolites are highly magnetized rocks compared to sedimentary rocks and one expects to have an almost zero depth to magnetic basement over ophiolite outcrops. Depth of magnetic basement is ~ 4 km over the outcrops of Kermanshah ophiolites (Compare **Figure 1a** with **Figure 2b**). Based on this observation, we speculate that the Kermanshah ophiolites constitute a very thin layer of highly magnetized rocks which has been thrusted over a ~4 km thick sedimentary cover (Chen et al., 2016; Teknik & Ghods, 2016). The recent 3D Pg velocity tomography map of NW Iran (Maheri-Peyrov et al., 2018) also show slow Pg velocity (i.e., not in the range of velocity of upper crustal crystalline rocks) of the upper crust within the region around Kermanshah ophiolites. This indirectly implies that the high P velocity ophiolitic rocks are too thin to increase the average velocity of the sedimentary cover.

To the NE of the MRF, the thickness of the sedimentary cover from the RF section (Chen et al.,

2016) is in agreement with the depth to magnetic basement (Teknik and Ghods, 2017). The 2D density model (**Figure 6**) shows the presence of the huge Bijar sedimentary basin to the NW of MRF and shows that this basin has a maximum thickness of the sedimentary cover of ~12 km thick. Based on the map of depth to magnetic basement in Iran (Teknik and Ghods, 2017), the Bijar sedimentary basin trends NW-SE and covers a 100 by 300 km large region (**Figure 2b**). From the margin of the newly discovered Bijar basin to the Tarom valley (profile distance 350-600 km), the thickness of the sedimentary cover decreases to less than 7 km (**Figure 2b** and **Figure 3**). The thickness of sedimentary cover from the Tarom valley to the NE end of the profile gradually increases to a maximum value of 15 km at the Caspian Sea, in agreement with the previous studies (Brunet et al., 2003; Mangino and Preistley, 1998).

Main Recent Fault (suture Zone): The Main Recent Fault (MRF) is traced at depth as a northeastward low angle dipping interface in the RF section (**Figure 3**). The negative converter in the RF model indicates a low P-wave velocity below the fault zone implying the presence of a shear zone at the MRF. The interpreted MRF has a gentle dip of ~13°, and it extends to a depth of ~35 km over ~150 km horizontal distance away from its surface trace. The gravity data has insufficient resolution to identify a possible low/density within the shear zone, and the magnetic data does not indicate any magma migration along the shear zone and identfied in other locations (Lyngsie and Thybo, 2007).

South Caspian basin crust: The 2D density model (**Figure 6**) includes a thin SCB crystalline crust (20 to 25 km) in the NE of the profile, which is overlain by a 15 km thick sedimentary cover. The interior of the SCB has been proposed to be formed by an oceanic-like crust (Mangino and Preistley, 1998). Our density model shows that the thin crystalline crust of SCB has an average

density of 2800 kg/m^3 and thus suggests a thinned and extended continental type of crust for the part of SCB crust in NE of the profile. We find that assigning a typical oceanic crust density to the SCB crust leads to a calculated Bouguer gravity anomaly, which is about 100 mGal larger than observed. Furthermore, the low magnetic anomaly (**Figure 4**) over the SCB part of the profile and the low susceptibility of the SCB igneous crust (**Figure 7**) also do not support an oceanic origin. Oceanic crust is much more magnetized than continental crust (e.g. Clark and Emerson, 1991; Hunt et al., 1995).

Moho step beneath the Tarom valley: The depth to the strongest converter abruptly decreases from ~50 km in Central Iran to ~30 km in the SCB (distance profile of ~480 km) which could suggest a steep change in Moho depth. Vertical Moho steps are generally expected to indicate major faults or sutures (e.g., Allam et al., 2017; Schulte-Pelkum and Ben-Zion, 2012). The suggested abrupt 20 km vertical offset of the Moho is in agreement with the variations in magnetic anomalies and topography (**Figure 4**) and the depth of seismicity (Aziz Zanjani et al., 2013; Ghods A. et al., 2016). The 80 km long surface rupture of the destructive Rudbar-Tarom 7.3 Mw 1990 event (Berberian and Walker, 2010) is located very close to the vertical offset of the Moho. We suggest that the sharp vertical offset of the strong converter is related to a suture zone between the northern limit of Alborz and the SCB crust, in contrast to previous studies which interpret the Khazar fault as the transition zone between the South Caspian basin and the Central Iran blocks (e.g, Allen et al., 2003; Guest et al., 2007; Şengör et al., 1984). The RF section (Chen et al., 2016) does not confirm any evidence of major faulting along the proposed Khazar fault similar to the negative dipping converter observed for the MRF (Chen et al., 2016; Paul et al., 2010).

We speculate that the converter step may indicate a Moho step which represents a Paleotethyan

suture zone. Remnants of the Paleotethys suture was first recognized in the NE of the Iranian plateau (Alavi, 1991) and lithological similarities suggest that the suture continues towards central and western Alborz near the Rasht ophiolitic unit (Alavi, 1996). Rossetti et al. (2017) suggest that the metamorphic rocks of the Rasht ophiolites form part of the Paleotethyan suture in Iran and can be interpreted as an exhumed subduction complex formed during Early Carboniferous oceanic subduction and subsequent Permian–Triassic suturing. Additionally, our density model indicates the presence of a body with intermediate density between normal lower crust and mantle at the step. This indicates that the present Moho is at the deep, weak converter around 55 km depth, but does not rule out that the original Moho has been offset in relation to tectonics during the Tethys collisions.

High density lower crust: Based on seismological and petrological studies, the lower crust is globally composed of high-density mafic rocks with a density range of $2900 < \rho < 3000$ kg/m^3 (Christensen and Mooney, 1995; Rudnick and Fountain, 1995). Generally, the trade-off between Moho depth and lower crustal density leads to non-uniqueness of these parameters. However, the ambiguity for the density of the lower crust is reduced by the a' priori constrained Moho depth from the receiver function model. The relatively large Bouguer anomaly above the thick crust in the ZTFB requires the presence of an anomalously high-density lower crust (3050 kg/m^3). Likewise, high crustal density of 3100 kg/m^3 is required below the Alborz Mountains (**Figure 5** and **Figure 6**). The very strong positive converter at depths around ~40 km beneath Zagros and Alborz implies a lower crustal layer with very high velocity. The high density layer may reflect partial eclogitization of the lower crust as has been suggested for Himalaya (Hetényi et al., 2007; Schulte-Pelkum et al., 2005) and other active and former orogenies (e.g., Abramovitz and Thybo, 2000; Sobolev and Babeyko, 2005),

The Zagros 2003 seismic profile (Paul et al., 2010) in the southern part of the Lurestan arc led to similar speculations about the actual Moho depth. The strong positive converter extends a distance of about 150 on the tip of the Arabian plate and extends to depths larger than ~40 km. The maximum thickness of the high velocity lower crust is about 20 km which is very similar to our observation. This could indicate that the high density lower crust may be present everywhere where the Arabian plate descends to depths deeper than 40 km. However, the Zagros 2001 profile (Paul et al., 2010) in Central Zagros does not have sufficient resolution for identification of the strong positive lower crustal converter.

Deeper density variations: Different researchers using different methodologies suggest thicker lithosphere beneath Zagros than the rest of the Iranian Plateau (e.g. Hafkenscheid et al., 2006; Paul et al., 2010; Priestley et al., 2012) and others (e.g. Hafkenscheid et al., 2006) also suggest deeper high velocity regions as relicts of the subducted Arabian plate. To investigate fully the style of deformation due to the continental collision in Iran, we should calculate the depth to the lithosphere-asthenosphere boundary (LAB) along our profile. However, our final density model explains the entire gravity signal which precludes calculation of variation in depth to the LAB.

6. Conclusions

We have documented and discussed a new gravity and magnetic susceptibility model of the NW part of the Iranian plateau along a recently acquired seismic profile across the Lurestan part of Zagros, Sanandaj-Sirjan Zone (SSZ), the Tertiary magmatic arcs, the Central Iran block, the Alborz Mountains, and the South Caspian Basin (**Figure 8**).

The thickness of the sedimentary cover is ~8 km in the Zagros fold and thrust belt (ZFTB) and the central Iran block, ~12 km in the Sanandaj-Sirjan Zone (SSZ) including the recently recognized

Bijar basin (Teknik and Ghods, 2017), and ~15 km in the South Caspian basin. The magnetic susceptibility model indicates that the Tertiary magmatic arcs at the northern edge of Central Iran are extruded or thrust over the sedimentary cover, the Kermanshah ophiolites form only a thin layer over a thick sedimentary cover, and the Qorveh intrusion is located within the Bijar sedimentary basin.

Around the Tarom valley a ~20 km thick high density lower crust is detected at the base end of the hitherto unidentified Palaeotethis suture. Also the lower crust below the Main recent fault has high density, indicative of partial eclogitization of the lower crust or the presence of a magmatic underplate. The crystalline crust of the ZFTB, the SSZ and the CI includes three layers, with a uniform thickness of ~20 km in the middle crust. The thickness of the upper crust increases from ~10 km in the ZFTB to ~15 km in the Central Iran block. The thickness of the high-density lower crust varies from ~15 in the ZFTB to ~25 km at the MRF. The SCB has a ~38 km thick crust, which include a ~15 km thick sedimentary cover, a ~18 km thick upper crust and a ~5 km thick lower crust. Neither density nor magnetic susceptibility data support an oceanic type of crust in this region. We propose the existence of a Palaeotethys related suture located ~50 km south of the Khazar fault between the Alborz Mountains and the South Caspian Basin. Our model provides a new tectonic framework for geodynamic understanding of the region and changes the widely accepted view about the borders of South Caspian Basin along the Khazar fault.

Acknowledgments:

This work was supported by grants from IASBS and a grant from Copenhagen University which financed the PhD studies by Vahid Teknik. Irina Artemieva gratefully acknowledges research grant DFF-1323-00053 from the Danish Fund for Independent Research. The receiver function

data related to CIGSIP seismic network in NW Iran was financially supported by the Strategic Priority Research Program of the Chinese Academy of Sciences (Grant No. XDB03010802). We acknowledge valuable comments from Khalil Motaghi, Esmaeil Shabanian, Mehdi Maheri and two anonymous reviewers.

7. References

Abramovitz, T., Thybo, H., 2000. Seismic images of Caledonian, lithosphere-scale collision structures in the southeastern North Sea along Mona Lisa Profile 2. Tectonophysics 317, 27–54. doi:10.1016/S0040-1951(99)00266-8

Agard, P., Omrani, J., Jolivet, L., Whitechurch, H., Vrielynck, B., Spakman, W., Monie, P., Meyer, B., Wortel, R., 2011. Zagros orogeny: a subduction-dominated process. Geol. Mag. 148, 692–725. doi:10.1017/S001675681100046X

Alavi, M., 1996. Tectonostratigraphic synthesis and structural style of the Alborz Mountain System in Iran. J. Geodyn. 21, 1–33.

Alavi, M., 1991. Sedimentary and structural characteristics of the Paleo-Tethys remnants in northeastern Iran. Geol. Soc. Am. Bull. 103, 983–992.

Alinaghi, A., Koulakov, I., Thybo, H., 2007. Seismic tomographic imaging of P- and S-waves velocity perturbations in the upper mantle beneath Iran. Geophys. J. Int. 169, 1089-1102.

Allam, A.A., Schulte-Pelkum, V., Ben-Zion, Y., Tape, C., Ruppert, N., Ross, Z.E., 2017. Ten kilometer vertical Moho offset and shallow velocity contrast along the Denali fault zone from double-difference tomography, receiver functions, and fault zone head waves. Tectonophysics 721, 56–69. doi:10.1016/j.tecto.2017.09.003

Amante, C., Eakins, B.W., 2009. ETOPO1 1 Arc-Minute Global Relief Model: Procedures, Data Sources and Analysis, NOAA Technical Memorandum NESDIS NGDC-24. doi:10.1594/PANGAEA.769615

Artemieva, I.M., Thybo, H., 2013. EUNAseis: A seismic model for Moho and crustal structure in Europe, Greenland, and the North Atlantic region. Tectonophysics 609, 97–153. doi:10.1016/j.tecto.2013.08.004

Aziz Zanjani, A., Ghods, A., Sobouti, F., Bergman, E., Mortezanejad, G., Priestley, K., Madanipour, S., Rezaeian, M., 2013. Seismicity in the western coast of the South Caspian Basin and the Talesh Mountains. Geophys. J. Int. 195, 799–814. doi:10.1093/gji/ggt299

Bavali, K., Motaghi, K., Sobouti, F., Ghods, A., Abbasi, M., Priestley, K., Mortezanejad, G., Rezaeian, M., 2016. Lithospheric structure beneath NW Iran using regional and teleseismic travel-time tomography. Phys. Earth Planet. Inter. 253, 97–107. doi:10.1016/j.pepi.2016.02.006

Berberian, F., Berberian, M., 1981. Tectono-plutonic episodes in Iran. pp. 5–32. doi:10.1029/GD003p0005

554 Berberian, M., 1995. Master "blind" thrust faults hidden under the Zagros folds: active basement tectonics
555 and surface morphotectonics. Tectonophysics. doi:10.1016/0040-1951(94)00185-C

556 Berberian, M., King, G.C.P., 1981. Towards a paleogeography and tectonic evolution of Iran. Can. J. Earth
557 Sci. 18, 210–265. doi:10.1139/e81-019

558 Berberian, M., Walker, R., 2010. The Rudbār Mw 7.3 earthquake of 1990 June 20; seismotectonics,
559 coseismic and geomorphic displacements, and historic earthquakes of the western 'High-Alborz',
560 Iran. Geophys. J. Int. 182, 1577–1602. doi:10.1111/j.1365-246X.2010.04705.x

561 Bouligand, C., Glen, J.M.G., Blakely, R.J., 2009. Mapping Curie temperature depth in the western United
562 States with a fractal model for crustal magnetization. J. Geophys. Res. Solid Earth 114, 1–25.
563 doi:10.1029/2009JB006494

564 Brunet, F.F., Korotaev, M. V., Ershov, A. V., Nikishin, A.M., 2003. The South Caspian Basin: A review of
565 its evolution from subsidence modelling. Sediment. Geol. 156, 119–148. doi:10.1016/S0037-
566 0738(02)00285-3

567 Casciello, E., Vergés, J., Saura, E., Casini, G., Fernández, N., Blanc, E., Homke, S., Hunt, D.W.W., 2009.
568 Fold patterns and multilayer rheology of the Lurestan Province, Zagros Simply Folded Belt (Iran). J.
569 Geol. Soc. London. 166, 947–959. doi:10.1144/0016-76492008-138

570 Chakravarthi, V., 1995. Gravity interpretation of nonoutcropping sedimentary basins in which the density
571 contrast decreases parabolically with depth. pure Appl. Geophys. 145, 327.

572 Chen, L., Jiang, M., Talebian, M., Ghods, A., Chung, S.-L., Ai, Y., Sobouti, F., He, Y., Motaghi, K.,
573 Zheng, T., Faridi, M., Chen, Q.-F., Lyu, Y., Xiao, W., Khalatbari Jafari, M., Zhu, R., 2016. New
574 Seismic Array Observation in the Northwestern Iranian Plateau, in: Geophysical Research Abstracts.
575 EGU, pp. 2016–3427.

576 Christensen, N.I., Mooney, W.D., 1995. Seismic velocity structure and composition of the continental
577 crust: A global view. J. Geophys. Res. doi:10.1029/95JB00259

578 Clark, D.A., Emerson, D.W., 1991. Notes on rock magnetization characteristics in applied geophysical
579 studies. Explor. Geophys. 22, 547–555. doi:10.1071/EG991547

580 Ekström, G., M. Nettles, and A. M. Dziewonski, 2012.The global CMT project 2004-2010: Centroid-
581 moment tensors for 13,017 earthquakes, Phys. Earth Planet. Inter., 200-201, 1-9,
582 doi:10.1016/j.pepi.2012.04.002

583 Emami, H., Vergés, J., Nalpas, T., Gillespie, P., Sharp, I., Karpuz, R., Blanc, E.P., Goodarzi, M.G.H., 2010.
584 Structure of the Mountain Front Flexure along the Anaran anticline in the Pusht-e Kuh Arc (NW
585 Zagros, Iran): insights from sand box models. Geol. Soc. London, Spec. Publ. 330, 155–178.
586 doi:10.1144/SP330.9

587 Engdahl, E.R., Jackson, J.A., Myers, S.C., Bergman, E.A., Priestley, K., 2006. Relocation and assessment
588 of seismicity in the Iran region. Geophys. J. Int. 167, 761–778. doi:10.1111/j.1365-
589 246X.2006.03127.x

590 Ghods A., Sobouti, F., Shabanian, E., Motaghi, K., 2016. Where are the boundaries of South Caspian
591 Basin. 34th National and 2th International Geosciences Congress., Tehran.

592 Gritto, R., Sibol, M.S., Siegel, J.E., Ghalib, H.A., Chen, Y., Herrmann, R.B., Alequabi, G.I., Tkalcic, H.,
593 Ali, B.S., Saleh, B.I., Mahmood, D.S., Shaswar, O.K., Mahmood, A., Abdullah, S., Ibrahim, F.,

Zand, R., Ali, B., Omar, L., Aziz, N.I., Ahmed, N.H., Al-nasiri, T., Ali, A.A., Taqi, A.A., Khalaf, S.R., 2008. Crustal structure of North Iraq from receiver function analyses, 2008 monitoring research review: ground-based nuclear explo- sion monitoring technologies. doi:FA8718–07-C-0008

Guest, B., Guest, A., Axen, G., 2007. Late Tertiary tectonic evolution of northern Iran: A case for simple crustal folding. Glob. Planet. Change 58, 435–453. doi:10.1016/j.gloplacha.2007.02.014

Hafkenscheid, E., Wortel, M.J.R., Spakman, W., 2006. Subduction history of the Tethyan region derived from seismic tomography and tectonic reconstructions. J. Geophys. Res. 111, B08401. doi:10.1029/2005JB003791

Hatzfeld, D., Molnar, P., 2010. Comparisons of the kinematics and deep structures of the Zagros and Himalaya and of the Iranian and Tibetan plateaus and geodynamic implications. Rev. Geophys. 48. doi:10.1029/2009RG000304

Hatzfeld, D., Tatar, M., Priestley, K., Ghafory-Ashtiany, M., 2003. Seismological constraints on the crustal structure beneath the Zagros Mountain belt (Iran). Geophys. J. Int. 155, 403–410. doi:10.1046/j.1365-246X.2003.02045.x

Hessami, K., Jamali, Tabassi, 2003. Major Active Faults of Iran. Remote Sens. Environ. doi:10.1016/j.rse.2007.08.025

Hetényi, G., Cattin, R., Brunet, F., Bollinger, L., Vergne, J., Nábělek, J.L., Diament, M., 2007. Density distribution of the India plate beneath the Tibetan plateau: Geophysical and petrological constraints on the kinetics of lower-crustal eclogitization. Earth Planet. Sci. Lett. 264, 226–244. doi:10.1016/j.epsl.2007.09.036

Hunt, C.P., Moskowitz, B.M., Banerjee, S.K., 1995. Rock Physics & Phase Relations: A Handbook of Physical Constants. AGU Ref. Shelf 3, 189–204. doi:10.1029/RF003

Jackson, J., Priestley, K., Allen, M., Berberian, M., 2002. Active tectonics of the South Caspian Basin. Geophys. J. Int. 148, 214–245. doi:10.1046/j.1365-246X.2002.01588.x

Jiang, M., Chen, L., Talebian, M., Ghods, A., Ai, Y., Sobouti, F., He, Y., Motaghi, K., Chen, Q.-F., Lyv, Y., Xiao, W., 2016. Fine Crustal Structure in the Northwestern Iranian Plateau Revealed by Ambient Noise Tomography, in: EGU General Assembly.

Jimenez-Munt, I., Fernandez, M., Saura, E., Verges, J., Garcia-Castellanos, D., 2012. 3-D lithospheric structure and regional/residual Bouguer anomalies in the Arabia-Eurasia collision (Iran). Geophys. J. Int. 190, 1311–1324. doi:10.1111/j.1365-246X.2012.05580.x

Lyngsie, S.B., Thybo, H., Rasmussen, T.M., 2006. Regional geological and tectonic structures of the North Sea area from potential field modelling. Tectonophysics 413, 147–170. doi:10.1016/j.tecto.2005.10.045

Lyngsie, S.B., Thybo, H., 2007. A new tectonic model for the Laurentia-Avalonia-Baltica sutures in the North Sea: A case study along MONA LISA profile 3. Tectonophysics 429, 201-227.

Maheri-Peyrov, M., Ghods, A., Donner, S., 2018. Crustal structure of NW Iran revealed by 3D Pg velocity tomography. Manuscr. Prep.

Malekzade, Z., Bellier, O., Abbassi, M.R., Authemayou, C., 2016. The effects of plate margin inhomogeneity on the deformation pattern within west-Central Zagros Fold-and-Thrust Belt. Tectonophysics. doi:10.1016/j.tecto.2016.01.030

Mangino, S., Preistley, K., 1998. The crustal structure of the South Caspian region. Geophys. J. Int. 133, 630–648.

Maus, S., Dimri, V., 1995. Potential field power spectrum inversion for scaling geology. J. Geophys. Res. doi:10.1029/95JB00758

McQuarrie, N., 2004. Crustal scale geometry of the Zagros fold-thrust belt, Iran. J. Struct. Geol. doi:10.1016/j.jsg.2003.08.009

Motaghi, K., Shabanian, E., Kalvandi, F., 2017. Underplating along the northern portion of the Zagros suture zone, Iran. Geophys. J. Int. 210, 375–389. doi:10.1093/gji/ggx168

Motavalli Anbaran, S.-H., Zeyen, H., Brunet, M.-F., Ardestani, V.E., 2011. Crustal and lithospheric structure of the Alborz Mountains, Iran, and surrounding areas from integrated geophysical modeling. Tectonics 30, n/a-n/a. doi:10.1029/2011TC002934

Nasrabadi, a, Tatar, M., Priestley, K., Sepahvand, M.R., 2008. Continental Lithosphere Structure Beneath the Iranian Plateau , From Analysis of Receiver Functions and Surface Waves Dispersion. Engineering.

Nábělek, J., Hetényi, G., Vergne, J., Sapkota, S., Kafle, B., Jiang, M., Su, H., Chen, J., Huang, B.S., Mitchell, L., Sherstad, D., Arsenault, M., Baur, J., Carpenter, S., Donnahue, M., Myers, D., Tseng, T.L., Bardell, T., Vanhoudnos, N., Pandey, M., Chitrakar, G., Rajaure, S., Xue, G., Wang, Y., Zhou, S., Liang, X., Ye, G., Liu, C.C., Lin, J., Wu, C.L., Barstow, N., 2009. Underplating in the himalaya-tibet collision zone revealed by the Hi-CLIMB experiment. Science (80-.). 325, 1371–1374. doi:10.1126/science.1167719

Nogole-Sadat, M.A.A. and Almasian, M., 1993. Tectonic Map of Iran in 1:1000,000 Scale. Tehran.

Paterson Grant & Watson Limited(PGW), 1973. Continuous Reduction to the Pole (VaryRTP).

Paul, A., Hatzfeld, D., Kaviani, A., Tatar, M., Péquegnat, C., 2010. Seismic imaging of the lithospheric structure of the Zagros mountain belt (Iran). Geol. Soc. London, Spec. Publ. 330, 5–18. doi:10.1144/SP330.2

Paul, A., Kaviani, A., Hatzfeld, D., Vergne, J., Mokhtari, M., 2006. Seismological evidence for crustal-scale thrusting in the Zagros mountain belt (Iran). Geophys. J. Int. 166, 227–237. doi:10.1111/j.1365-246X.2006.02920.x

Priestley, K., McKenzie, D., Barron, J., Tatar, M., Debayle, E., 2012. The Zagros core: Deformation of the continental lithospheric mantle. Geochemistry, Geophys. Geosystems 13, 1–21. doi:10.1029/2012GC004435

Rahmani, M., Motaghi, K., Ghods, A., Sobouti, F., Talebian, M., Chen, L., Jiang, M., 2018. Tethyan subducted slab and seismic anisotropy in the upper mantle beneath the north Zagros collision using S teleseismic tomography, in: Proceedings of the 18th Iranian Geophysical Conference. pp. 471–473.

Rao, D.B., 1986. Modelling of sedimentary basins from gravity anomalies with variable density contrast. Geophys. J. Int. 84, 207–212. doi:10.1111/j.1365-246X.1986.tb04353.x

Richards, J.P., Şengör, A.M.C., 2017. Did Paleo-Tethyan anoxia kill arc magma fertility for porphyry copper formation? Geology 45, 591–594. doi:10.1130/G38954.1

673 Rossetti, F., Monié, P., Nasrabady, M., Theye, T., Lucci, F., Saadat, M., 2017. Early Carboniferous
674 subduction-zone metamorphism preserved within the Palaeo-Tethyan Rasht ophiolites (western
675 Alborz, Iran). J. Geol. Soc. London. 174, 741–758. doi:10.1144/jgs2016-130

676 Rudnick, R.L., Fountain, D.M., 1995. Nature and composition of the continental crust: A lower-crustal
677 perspective. Rev. Geophys. 33, 267–309. doi:Doi 10.1029/95rg01302

678 Saleh, R., 2006. Reprocessing of aeromagnetic map of Iran. Institute for Advanced Studies in Basic
679 Sciences.

680 Schulte-Pelkum, V., Ben-Zion, Y., 2012. Apparent vertical Moho offsets under continental strike-slip faults
681 from lithology contrasts in the seismogenic crust. Bull. Seismol. Soc. Am. 102, 2757–2763.
682 doi:10.1785/0120120139

683 Schulte-Pelkum, V., Monsalve, G., Sheehan, A., Pandey, M.R., Sapkota, S., Bilham, R., Wu, F., 2005.
684 Imaging the Indian subcontinent beneath the Himalaya. Nature 435, 1222–1225.
685 doi:10.1038/nature03678

686 Şengör, A.M.C., Yilmaz, Y., Sungurlu, O., 1984. Tectonics of the Mediterranean Cimmerides: nature and
687 evolution of the western termination of Palaeo-Tethys. Geol. Soc. London, Spec. Publ.
688 doi:10.1144/GSL.SP.1984.017.01.04

689 Sengor, A.M.C., Natalin, B.A., 1996. Turkic-type orogeny and its role in the making of the
690 continental crust. Annual Review of Earth and Planetary Sciences 24, 263-337

691 Sepehr, M., Cosgrove, J.W., 2004. Structural framework of the Zagros Fold-Thrust Belt, Iran. Mar. Pet.
692 Geol. doi:10.1016/j.marpetgeo.2003.07.006

693 Sobolev, S. V., Babeyko, A.Y., 2005. What drives orogeny in the Andes? Geology 33, 617–620.
694 doi:10.1130/G21557.1

695 Stocklin, J., 1968. Structural History and Tectonics of Iran: A Review. Am. Assoc. Pet. Geol. Bull. 52,
696 1229–1258.

697 Talebian, M., Jackson J., 2002. Offset on the Main Recent Fault of NW Iran and implications for the late
698 Cenozoic tectonics of the Arabia–Eurasia collision zone, Geophys. J. In, 150, Issue 2, 422–
699 439, doi:10.1046/j.1365-246X.2002.01711.x

700 Tatar, M., Hatzfeld, D., Ghafory-Ashtiany, M., 2004. Tectonics of the Central Zagros (Iran) deduced from
701 microearthquake seismicity. Geophys. J. Int. doi:10.1111/j.1365-246X.2003.02145.x

702 Tatar, M., Jackson, J., Hatzfeld, D., Bergman, E., 2007. The 2004 May 28 Baladeh earthquake (Mw 6.2) in
703 the Alborz, Iran: Overthrusting the South Caspian Basin margin, partitioning of oblique convergence
704 and the seismic hazard of Tehran. Geophys. J. Int. doi:10.1111/j.1365-246X.2007.03386.x

705 Tatar, M., Nasrabadi, A., 2013. Crustal thickness variations in the Zagros continental collision zone (Iran)
706 from joint inversion of receiver functions and surface wave dispersion. J. Seismol. 17, 1321–1337.
707 doi:10.1007/s10950-013-9394-z

708 Teknik, V., Ghods, A., 2017. Depth of magnetic basement in Iran based on fractal spectral analysis of
709 aeromagnetic data. Geophys. J. Int. 209, 1878–1891. doi:10.1093/gji/ggx132

710 Thybo, H., 2001. Crustal structure along the EGT profile across the Tornquist Fan interpreted from seismic,
711 gravity and magnetic data. Tectonophysics 334, 155–190. doi:10.1016/S0040-1951(01)00055-5

712 Thybo, H., Artemieva, I.M., 2013. Moho and magmatic underplating in continental lithosphere.
713 Tectonophysics 609, 605-619, doi:610.1016/j.tecto.2013.1005.1032.

714 Tunini, L., Jiménez-Munt, I., Fernandez, M., Vergés, J., Villaseñor, A., 2015. Lithospheric mantle
715 heterogeneities beneath the Zagros Mountains and the Iranian Plateau: A petrological-geophysical
716 study. Geophys. J. Int. 200, 596–614. doi:10.1093/gji/ggu418

717 Verdel, C., Wernicke, B.P., Hassanzadeh, J., Guest, B., 2011. A Paleogene extensional arc flare - up in
718 Iran. Tectonics 30, 1–20. doi:10.1029/2010TC002809

719 Vergés, J., Goodarzi, M., Emami, H., Karpuz, R., Efstathiou, J., Gillespie, P., 2011a. Multiple detachment
720 folding in Pusht-e Kuh arc, Zagros: Role of mechanical stratigraphy. Thrust fault-related Fold.
721 AAPG Mem. 69–94. doi:10.1306/13251333M942899

722 Vergés, J., Grelaud, S., Karpuz, R., Osthus, H., Nalpas, T., Sharp, I., Guadarzi, H., 2003. the Structure of
723 the Zagros Mountain Front (Se Lurestan , Iran): Controls From Multiple Detachment Levels.
724 Society 5, 5.

725 Vergés, J., Saura, E., Casciello, E., Fernandez, M., Villasenor, A., Jimenz-Munt, I., Garcia-Castellanos, D.,
726 2011b. Crustal-scale cross-sections across the NW Zagros belt: implications for the Arabian margin
727 reconstruction. Geol. Mag. 148, 739–761. doi:10.1017/S0016756811000331

728 Wu, Q., and Zeng, R.,1998. The crustal structure of Qinghai-Xizang plateau inferred from broadband
729 teleseismic waveform (in Chinese with English abstract), Chin. J. Geophys., 41, 669 – 679.

730 Zanchi, A., Zanchetta, S., Berra, F., Mattei, M., Garzanti, E., Molyneux, S., Nawab, A., Sabouri, J., 2009.
731 The Eo-Cimmerian (Late? Triassic) orogeny in North Iran. Geol. Soc. London, Spec. Publ. 312, 31–
732 55. doi:10.1144/SP312.3

733
734
735
736
737
738
739
740
741
742
743
744
745
746

List of figure captions

Figure 1: **a)** Topography of the Iranian plateau based on the ETOPO 1 global elevation model (Amante and Eakins, 2009). The solid straight line (AA') shows the location of the profile along which we model the crustal density and susceptibility distribution. Major active faults (Hessami et al., 2003) are shown as solid black lines. The thick grey, solid lines show political boundaries. Colored dots show earthquake epicenters of earthquakes between 1964 and 2017 on the Iranian Plateau (Engdahl et al., (2006) and, for the period of 1918-2004, new data from Iranian Seismological Center website (irsc.ut.ac.ir/bulletin.php;last download March 2017)). To assure a reasonable location accuracy, only events with azimuthal gap less than 120 degree are selected. The red star shows the location of the recent 7.3 Mw Sarpolzahab low angle thrust earthquake on 12 November 2017. The beachballs are from CMT Global focal mechanisms solutions (Ekström et al 2012) for events larger than magnitude 6 that happened between 1970 and present in the study area. **b)** Schematic cross-section of the regional tectonic setting based on commonly accepted models (e.g. 2004; Berberian and King, 1981; Paul et al., 2010; Stocklin, 1968). The crustal scale interaction between the lithospheric blocks of the Zagros, Central Iran (CI) and South Caspian basin (SCB) is caused by large scale regional compression associated with the Arabian-Eurasian (EUR) collision. Abbreviations: MRF - Main Recent Fault, HZF - High Zagros Fault, MFF - Mountain Frontal Fault, TF - Talesh Fault, T - Tarom Valley, KF - Khazar Fault, Talesh M. - Talesh Mountains. MRF - Main Recent Fault, SSZ - Sanandaj-Sirjan Zone, MMA - Mesozoic Magmatic Arc, and TMA - Tertiary Magmatic Arc.

Figure 2: a) Simplified tectonic map of the NW part of the Iranian plateau (modified from the structural map of the National Geoscience Database of Iran, NGDIR; http://www.ngdir.ir). Black lines show the active faults; circles RF Moho depths in the study region: Talesh (Bavali et al., 2016), CIGSIP receiver function profiles (Chen et al., 2016), EUNASeis dataset (Artemieva and Thybo, 2013), Zagros 2003 profile (Paul et al., 2010), NW Iraq receiver function study labeled "G" shown by diagonal left hatches (Gritto et al., 2008) and other scattered stations (Hatzfeld et al., 2003; Nasrabadi et al., 2008). **b)** Depth to the magnetic basement (Teknik and Ghods, 2017), with superimposed sediment thickness based on a structural study across the NW Zagros belt marked by squares (Vergés et al., 2011) and sediment thickness determined from seismic receiver function studies (circles) including the CIGSIP profile (Chen et al., 2016) and the Zagros 2003 (Paul et al., 2010). The recently discovered Bijar basin (Teknik and Ghods, 2017) is marked by the hatched polygon. **c)** Bouguer anomalies in the NW part of the Iranian plateau. The small black dots indicate gravity stations from Bureau Gravimétrique International (BGI, http://bgi.omp.obsmip.fr). Major active faults (Hessami et al., 2003) are shown as solid gray lines. **d)** Reprocessed Aeromagnetic intensity map of Iran (Saleh, 2006). The map is reduced to pole

using the continuous reduction to pole method (Paterson Grant & Watson Limited (PGW), 1973). Abbreviations: QA - Qorveh anomaly area (hatched polygon), ZFB - Zagros Fold Belt, CI - Central Iran block, AM - Alborz Mountains Tertiary Magmatic Arc. Positive magnetic anomalies PM1 and PM2 and negative magnetic anomalies NM1 and NM2 indicate magnetic anomalies with wavelengths longer than 150 km, which possibly are associated with deeper sources (see Figure 3). Abbreviations same as Figure 1.

Figure 3: density modeling Step 1: Top: Observed and computed Bouguer gravity anomaly along the profile (for location see **Figure 1a**). The observed anomaly is shown by a thick black line. Thin black line is the computed Bouguer anomaly and the thin red line is the misfit between the observed and calculated anomalies. Middle: All seismic interfaces extracted from the seismic RF model (Chen et al., 2016). Positive and negative interfaces are shown by black and red solid lines. The Moho interface is marked by a thick black line in the bottom of the model. Topography are shown by thick blue line. The depth to the first positive converter interface is shown by a green line. The depth to magnetic basement is shown as a thick pink line. Bottom: 2D density model with homogeneous density for the sedimentary succession, crystalline crust, and upper mantle. Vertical exaggeration (V.E.) is 1.7. ZFTB indicates Zagros fold and thrust belt and other abbreviations for the tectonic units are as in **Figure 1** and **2**.

Figure 4: Comparison of topography (solid black line), reduced to pole aeromagnetic anomaly (solid blue line), low pass 150 km filtered aeromagnetic anomaly (doted blue line), terrestrial gravity anomaly (solid red line) and satellite gravity anomaly (dashed red line) along the modeling profile. Positive magnetic anomalies PM1 and PM2 can be associated with a depressed Curie isotherm or a high susceptibility material with a shallower CDP. Negative magnetic anomalies NM1 and NM2 can be explained either by a thin magmatic layer or a by low susceptibility in the shallow crust. TMA stands for location of the Tertiary Magmatic Arc. Abbreviations for the tectonic units are described in **Figure 1** and **2**.

Figure 5: density modeling Step 2: In order to reduce the difference between the computed and the observed gravity anomalies (**Figure 3**), the crust is subdivided into more layers. The boundaries between these layers are based on the observed RF boundaries within the crust (middle part). Numbers 1 and 2 in the RF section (the middle panel) show the two possible alternatives Moho depths around the Tarom valley. The numbers represent the density values for each layer in kg/m^3. The dashed lines show the less reliable inferred boundaries.

Figure 6*:* Final density model (step 3): Top) Observed anomaly (bold line), calculated Bouguer anomaly (thin black line) and their difference (red line). Bottom) Crustal and upper mantle 2D density model. The crust primarily is divided into the sedimentary layer, the crystalline crust and the mantle. The sediment layer includes the upper, low density, and the lower, denser, part. The crystalline crust is divided into the upper, middle and lower parts.

Figure 7: Magnetic susceptibility models **a)** Susceptibility model with the Curie Depth Point (CDP) boundary at a constant depth of 40 km. The residual magnetic anomaly in the top panel (highlighted by thick gray line) includes long wavelength variations. **b)** The final magnetic susceptibility model in which the Curie isotherm boundary is allowed to vary. The model shows

shallowing of the CDP beneath the SSZ and the Alborz mountains at the two interpreted sutures along the profile. Black lines on the susceptibility models are from the density model (**Figure 6**). Red lines mark the CDP and the green line shows the sediment-basement boundary. The numbers in the susceptibility models show susceptibility of a given layer in SI units. Susceptibility of the sedimentary layer is assumed to be 0.001 SI and is fixed to zero at depths below the Curie isotherm. The numbers 1, 2, and 3 on the susceptibility models represent the Kermanshah ophiolite, Qorveh intrusion, and the Tertiary magmatic arc of Alborz, respectively.

Figure 8: Simplified sketch of the density and susceptibility models. Major boundaries: Green lines correspond to the sediment-basement boundary; Thick black line represents Moho and crustal scale faults, and solid dashed lines are the boundaries inferred from the density modeling.

Figures

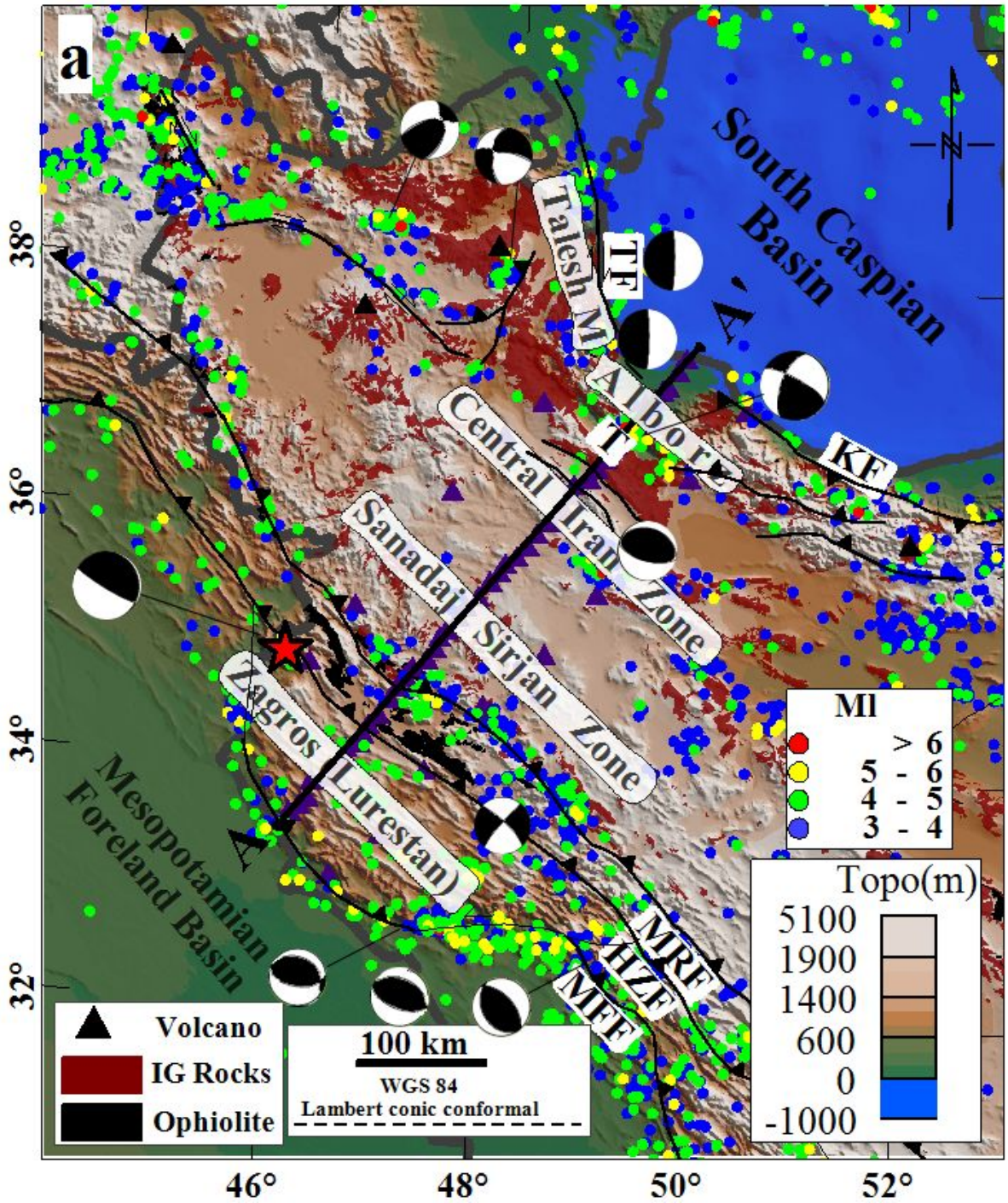

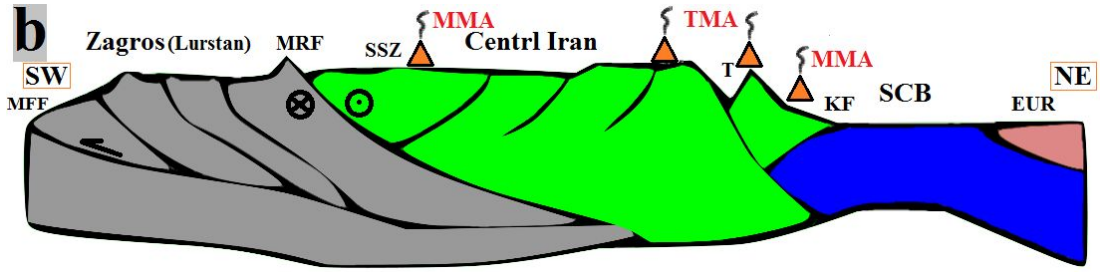

Figure 2: **a)** Topography of the Iranian plateau based on the ETOPO 1 global elevation model (Amante and Eakins, 2009). The solid straight line (AA') shows the location of the profile along which we model the crustal density and susceptibility distribution. Major active faults (Hessami et al., 2003) are shown as solid black lines. The thick grey, solid lines show political boundaries. Colored dots show earthquake epicenters of earthquakes between 1964 and 2017 on the Iranian Plateau (Engdahl et al., (2006) and, for the period of 1918-2004, new data from Iranian Seismological Center website (irsc.ut.ac.ir/bulletin.php;last download March 2017)). To assure a reasonable location accuracy, only events with azimuthal gap less than 120 degree are selected. The red star shows the location of the recent 7.3 Mw Sarpolzahab low angle thrust earthquake on 12 November 2017. The beachballs are from CMT Global focal mechanisms solutions (Ekström et al 2012) for events larger than magnitude 6 that happened between 1970 and present in the study area. **b)** Schematic cross-section of the regional tectonic setting based on commonly accepted models (e.g. 2004; Berberian and King, 1981; Paul et al., 2010; Stocklin, 1968). The crustal scale interaction between the lithospheric blocks of the Zagros, Central Iran (CI) and South Caspian basin (SCB) is caused by large scale regional compression associated with the Arabian-Eurasian (EUR) collision. Abbreviations: MRF - Main Recent Fault, HZF - High Zagros Fault, MFF - Mountain Frontal Fault, TF - Talesh Fault, T - Tarom Valley, KF - Khazar Fault, Talesh M. - Talesh Mountains. MRF - Main Recent Fault, SSZ - Sanandaj-Sirjan Zone, MMA - Mesozoic Magmatic Arc, and TMA - Tertiary Magmatic Arc.

868 .

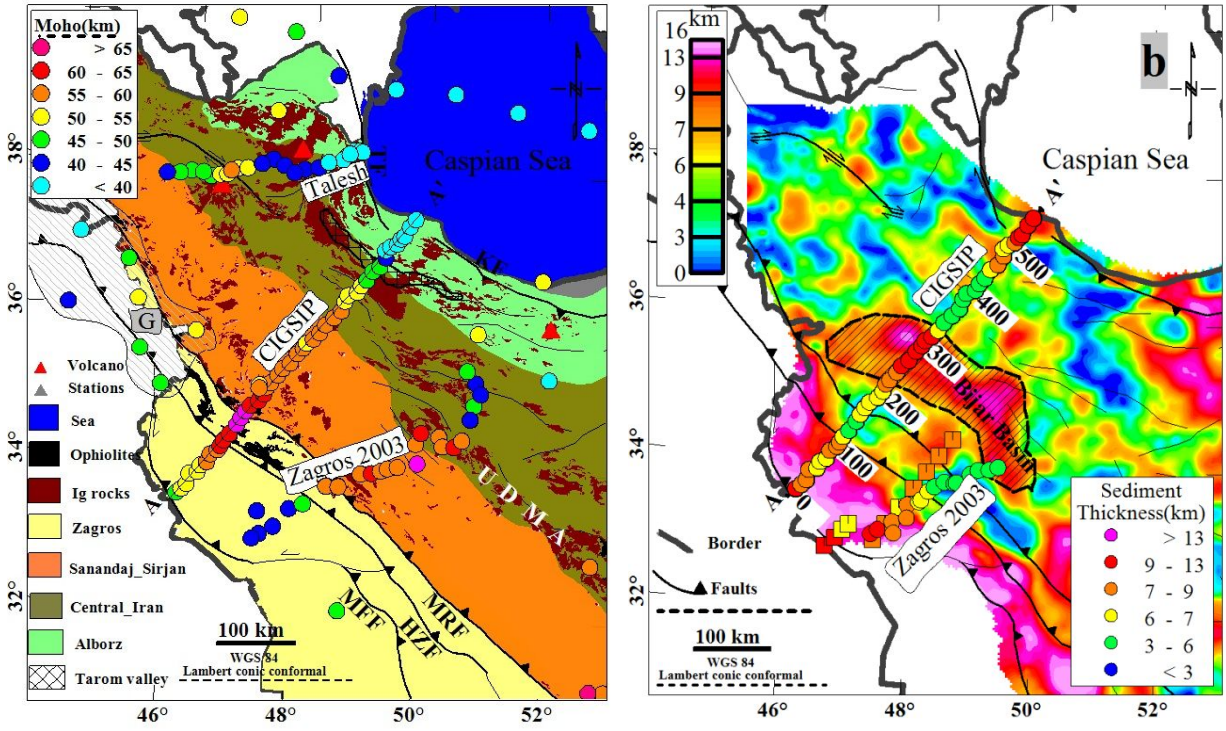

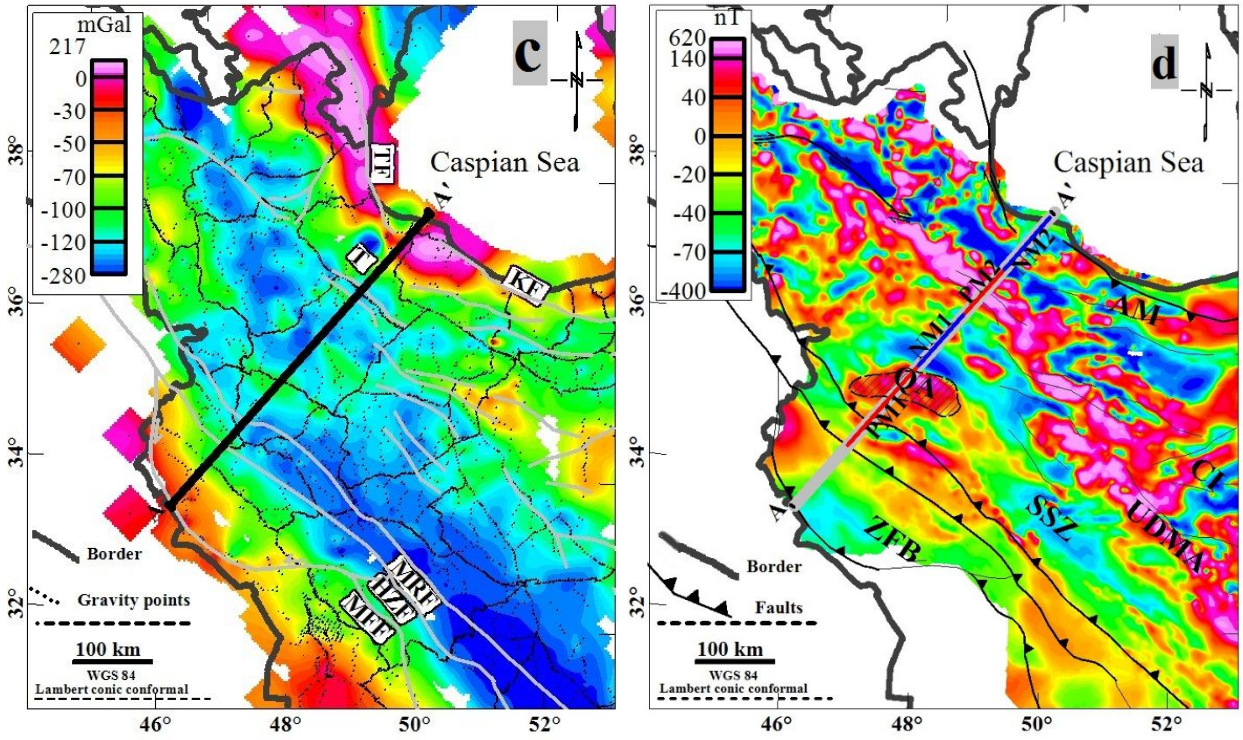

Figure 2: a) Simplified tectonic map of the NW part of the Iranian plateau (modified from the structural map of the National Geoscience Database of Iran, NGDIR; http://www.ngdir.ir). Black lines show the active faults; circles RF Moho depths in the study region: Talesh (Bavali et al., 2016), CIGSIP receiver function profiles (Chen et al., 2016), EUNASeis dataset (Artemieva and Thybo, 2013), Zagros 2003 profile (Paul et al., 2010), NW Iraq receiver function study labeled "G" shown by diagonal left hatches (Gritto et al., 2008) and other scattered stations (Hatzfeld et al., 2003; Nasrabadi et al., 2008). **b)** Depth to the magnetic basement (Teknik and Ghods, 2017), with superimposed sediment thickness based on a structural study across the NW Zagros belt marked by squares (Vergés et al., 2011) and sediment thickness determined from seismic receiver function studies (circles) including the CIGSIP profile (Chen et al., 2016) and the Zagros 2003 (Paul et al., 2010). The recently discovered Bijar basin (Teknik and Ghods, 2017) is marked by the hatched polygon. **c)** Bouguer anomalies in the NW part of the Iranian plateau. The small black dots indicate gravity stations from Bureau Gravimétrique

International (BGI, http://bgi.omp.obsmip.fr). Major active faults (Hessami et al., 2003) are shown as solid gray lines. **d)** Reprocessed Aeromagnetic intensity map of Iran (Saleh, 2006). The map is reduced to pole using the continuous reduction to pole method (Paterson Grant & Watson Limited (PGW), 1973). Abbreviations: QA - Qorveh anomaly area (hatched polygon), ZFB - Zagros Fold Belt, CI - Central Iran block, AM - Alborz Mountains Tertiary Magmatic Arc. Positive magnetic anomalies PM1 and PM2 and negative magnetic anomalies NM1 and NM2 indicate magnetic anomalies with wavelengths longer than 150 km, which possibly are associated with deeper sources (see Figure 3). Abbreviations same as Figure 1.

869 .

870 .

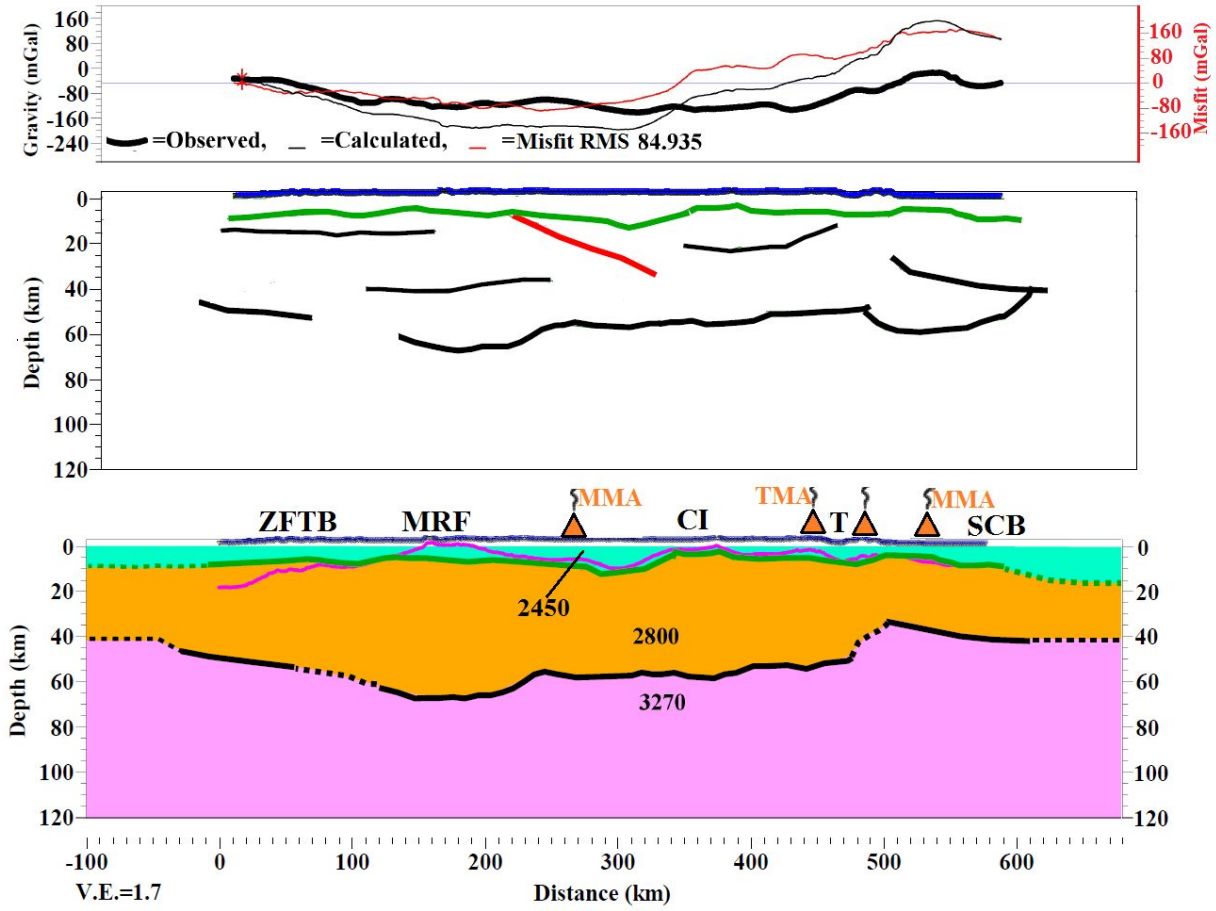

Figure 3: density modeling Step 1: Top: Observed and computed Bouguer gravity anomaly along the profile (for location see **Figure 1a**). The observed anomaly is shown by a thick black line. Thin black line is the computed Bouguer anomaly and the thin red line is the misfit between the observed and calculated anomalies. Middle: All seismic interfaces extracted from the seismic RF model (Chen et al., 2016). Positive and negative interfaces are shown by black and red solid lines. The Moho interface is marked by a thick black line in the bottom of the model. Topography are shown by thick blue line. The depth to the first positive converter interface is shown by a green line. The depth to magnetic basement is shown as a thick pink line. Bottom: 2D density model with homogeneous density for the sedimentary succession, crystalline crust, and upper mantle. Vertical exaggeration

(V.E.) is 1.7. ZFTB indicates Zagros fold and thrust belt and other abbreviations for the tectonic units are as in **Figure 1** and **2**.

871 .

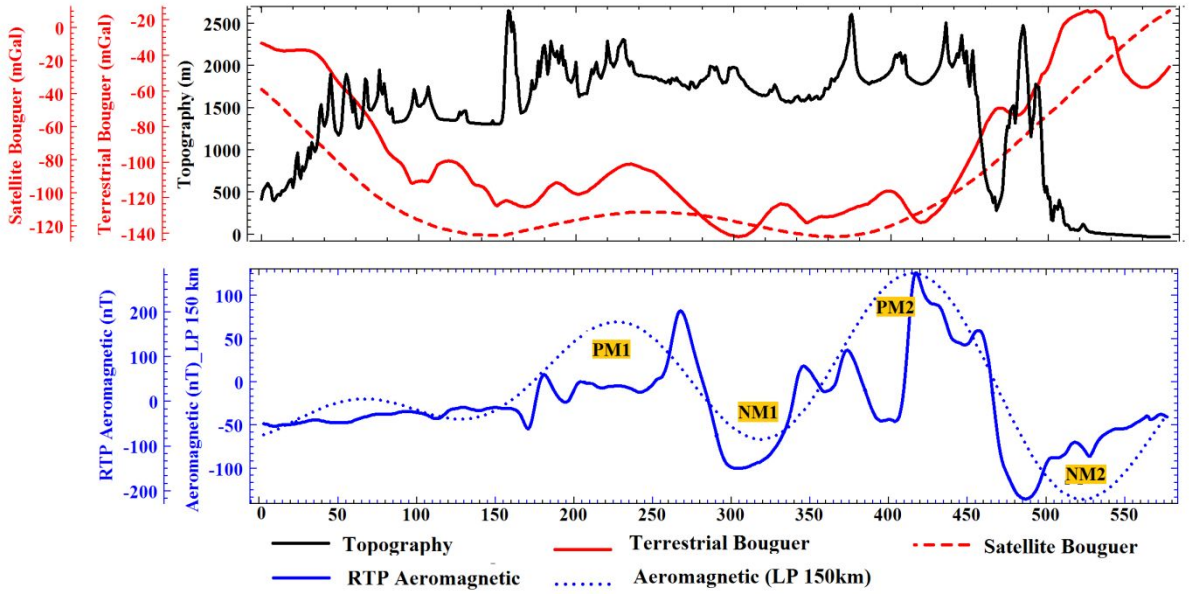

Figure 4: Comparison of topography (solid black line), reduced to pole aeromagnetic anomaly (solid blue line), low pass 150 km filtered aeromagnetic anomaly (doted blue line), terrestrial gravity anomaly (solid red line) and satellite gravity anomaly (dashed red line) along the modeling profile. Positive magnetic anomalies PM1 and PM2 can be associated with a depressed Curie isotherm or a high susceptibility material with a shallower CDP. Negative magnetic anomalies NM1 and NM2 can be explained either by a thin magmatic layer or a by low susceptibility in the shallow crust. TMA stands for location of the Tertiary Magmatic Arc. Abbreviations for the tectonic units are described in **Figure 1** and **2**.

872

873 .

874

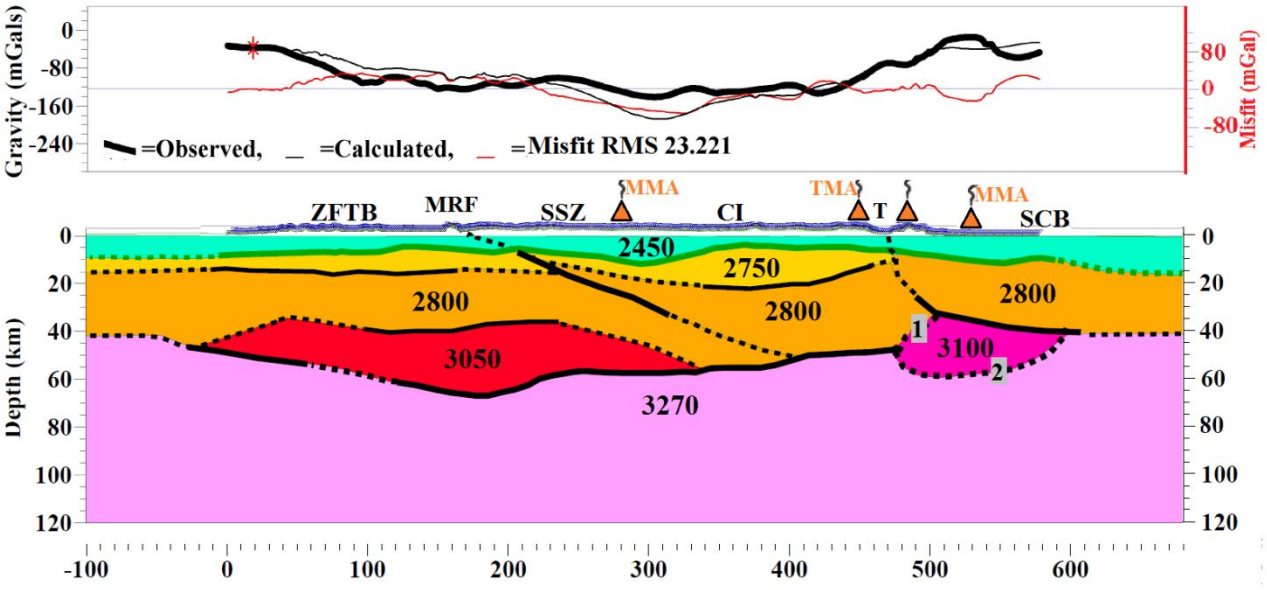

Figure 5: density modeling Step 2: In order to reduce the difference between the computed and the observed gravity anomalies (**Figure 3**), the crust is subdivided into more layers. The boundaries between these layers are based on the observed RF boundaries within the crust (middle part). Numbers 1 and 2 in the RF section (the middle panel) show the two possible alternatives Moho depths around the Tarom valley. The numbers represent the density values for each layer in kg/m^3. The dashed lines show the less reliable inferred boundaries.

875

876 .

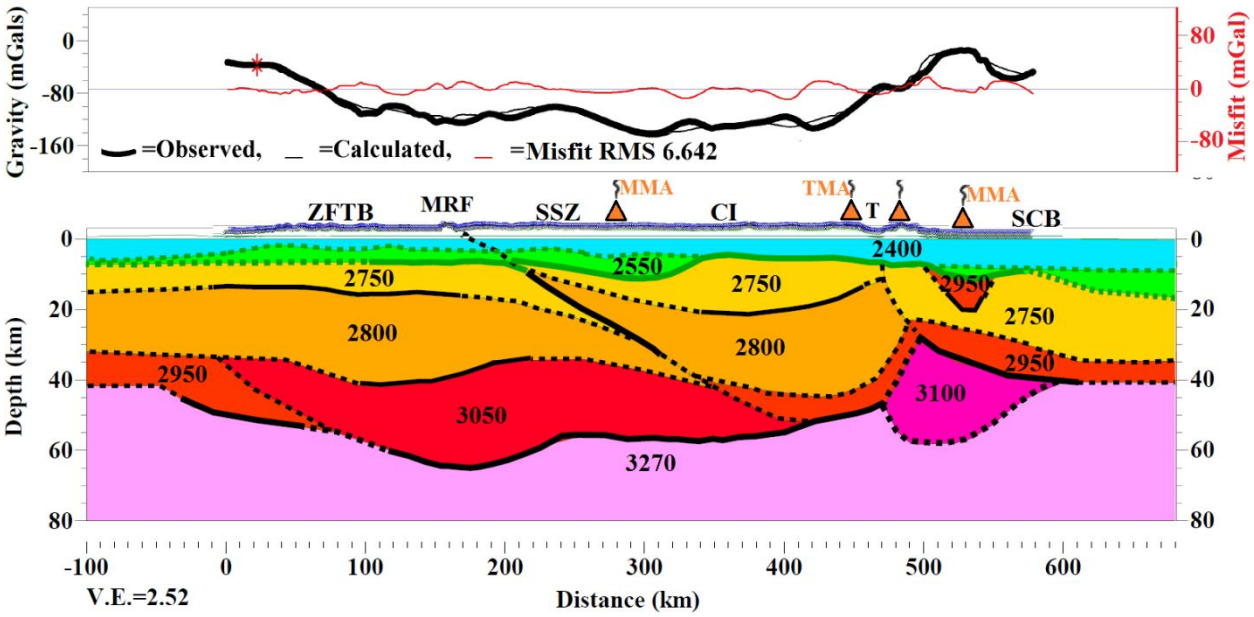

Figure 6*:* Final density model (step 3): Top) Observed anomaly (bold line), calculated Bouguer anomaly (thin black line) and their difference (red line). Bottom) Crustal and upper mantle 2D density model. The crust primarily is divided into the sedimentary layer, the crystalline crust and the mantle. The sediment layer includes the upper, low density, and the lower, denser, part. The crystalline crust is divided into the upper, middle and lower parts.

877 .

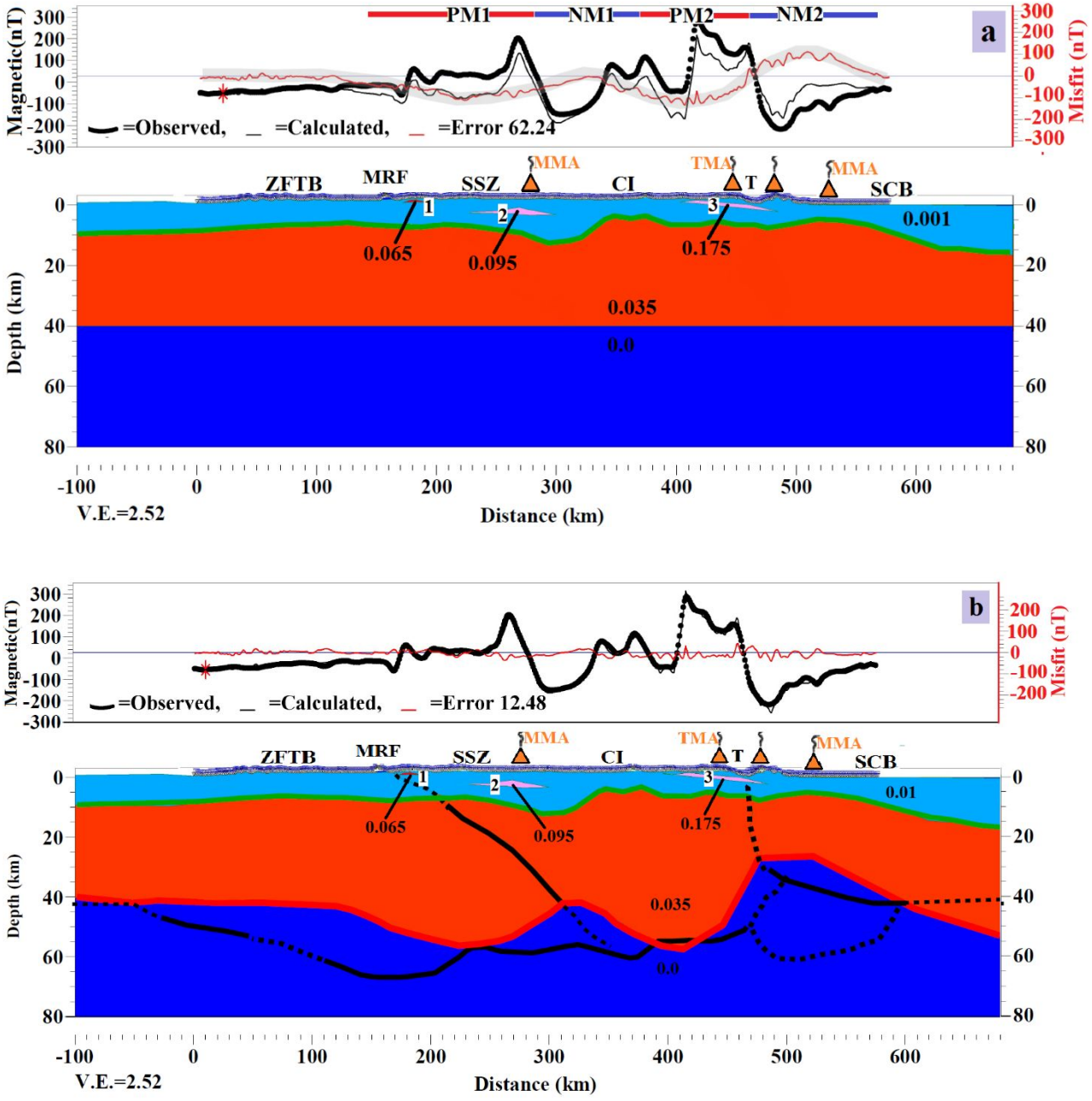

Figure 7: Magnetic susceptibility models **a)** Susceptibility model with the Curie Depth Point (CDP) boundary at a constant depth of 40 km. The residual magnetic anomaly in the top panel (highlighted by thick gray line) includes long wavelength variations. **b)** The final magnetic susceptibility model in which the Curie isotherm boundary is allowed to vary. The model shows shallowing of the CDP

beneath the SSZ and the Alborz mountains at the two interpreted sutures along the profile. Black lines on the susceptibility models are from the density model (**Figure 6**). Red lines mark the CDP and the green line shows the sediment-basement boundary. The numbers in the susceptibility models show susceptibility of a given layer in SI units. Susceptibility of the sedimentary layer is assumed to be 0.001 SI and is fixed to zero at depths below the Curie isotherm. The numbers 1, 2, and 3 on the susceptibility models represent the Kermanshah ophiolite, Qorveh intrusion, and the Tertiary magmatic arc of Alborz, respectively.

878 .

879 .

880

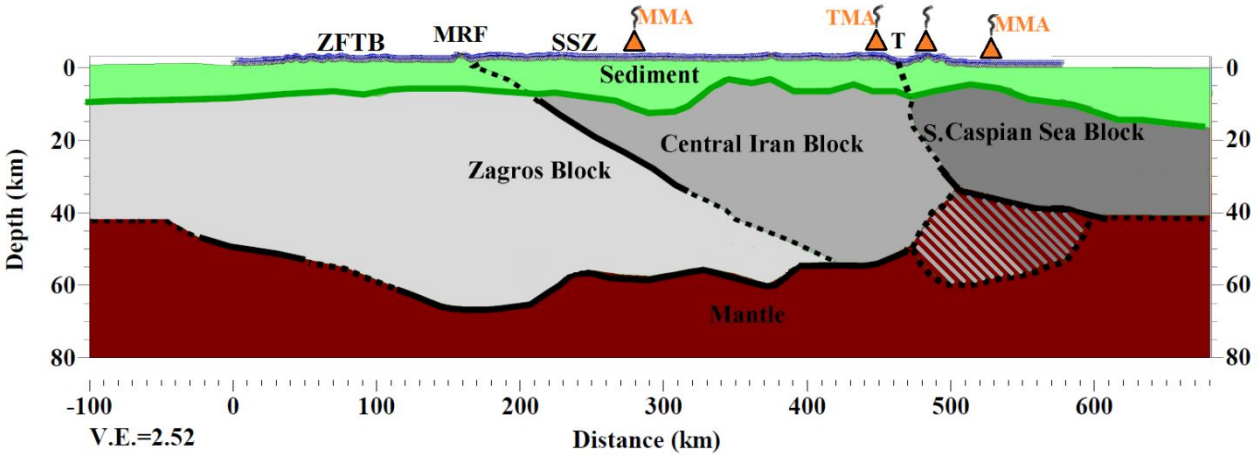

Figure 8: Simplified sketch of the density and susceptibility models. Major boundaries: Green lines correspond to the sediment-basement boundary; Thick black line represents Moho and crustal scale faults, and solid dashed lines are the boundaries inferred from the density modeling.

Appendix A1: Sensitivity Analyze of density model.

To address possible non-uniqueness of the gravity model presented in **Figure 6**, we test the sensitivity of the density model in relation to key parameters, including the Caspian dense shallow body, the upper, middle and lower crust, Zagros root and Alborz root. The sensitivity analyses were undertaken to understand how density variations within plausible ranges may affect the response of the density model. The density of the mentioned crustal units have been limited to the range of density values derived froma compilation of seismic studies (i.e. Artemieva and Thybo, 2013). Sensitivity of the model to density of a particular crustal unit is assessed systematically by varying the density and calculating the response of the model. Crustal units with a high sensitivity on density are strongly influenced by density variations and thus are less ambiguous than other parameters.

Figure A1 shows the response of the gravity model for different density values (Table A1) assigned to the shallow high density Caspian body. The sensitivity analysis shows that a dense source in the upper Caspian crust is necessary in the northern end of the profile. Figure A1 shows strong gravity response with respect with density variations of the body and suggests a density in the range of 2950 to 3000 kg/m^3 for the shallow seated body. The experiment vividly shows that a density value in the range of normal upper crustal values (Test number 1 in the table A1) cannot reproduce the short gravity wavelength. The Bouguer gravity map (**Figure 2c**) shows a high amplitude short wavelength Bouguer anomaly along the south and southwest borders of the Caspian Sea. We speculate that the high amplitude short wavelength Bouguer anomaly is due to shallow seated mafic rocks.

916 Figure A2 shows the response of the gravity model for different density values (Table A2) for the
917 Alborz root which is shown by purple color beneath Tarom valley in **Figure 6**. Figure A2 clearly
918 shows that the response of the crustal root of Alborz is strongly dependent on the density and give
919 the minimum misfit for the adopted density of 3100 kg/m^3, the value used already in our density
920 model.

921 Figure A3 display the response of the gravity model for different density values (Table A3) for the
922 Zagros root which is shown by purple color beneath Zagros in **Figure 6**. As for Alborz, Figure A3
923 clearly shows that the response of the crustal root of Zagros is strongly dependent on the density
924 and gives the minimum misfit for the adopted density of 3050 kg/m^3, the value used in our density
925 model.

926 The models presented in Figure A3 shows that the gravity response of the model strongly changes
927 with density of the crustal root, also in the Alborz region. This observation casts serious doubt on
928 the possible existence of a tradeoff between the density of the Alborz and Zagros root. To
929 investigate this possible source of non-uniqueness, we calculate the gravity response of our model
930 using 36 combinations for density of the crustal root of Alborz and Zagros as listed in Table A4.
931 Figure A4 shows that the lowest misfit is for a density of 3050 kg/m^3 for the Zagros root and 3100
932 kg/m^3 for the Alborz root, as already used in our model (**Figure 6**).

933 In the fifth stage of sensitivity analysis, we investigate possible tradeoff between density of the
934 upper, middle and lower crust and the dense Alborz and Zagros roots. Table A5 describes the
935 tested models. The results indicate that the differences in density of the two roots for Zagros and
936 Alborz is necessary and furthermore a relatively denser root for the Alborz mountains is required
937 with respect to the Zagros root.This indicates that the Bouguer anomaly over Zagros could not

equally be caused by increasing density through the whole crust.

In the final sensitivity analysis, we want to investigate the possibility of fitting the observed gravity by changing the geometry of the lower crust while the density of all the shallower units are the same as those used in Figure 6 but the density of the lower crust is fixed to 2950 kg/m^3 (i.e., no dense crustal root is considered). With this test we would like to decipher if a small change in the depth of the boundaries of the lower crust could remove the necessity of having the dense crustal root. If the changes in the depth of boundaries are of the order of uncertainty in the RF image there would be no need to include a dense lower crustal root. Using an inversion scheme (Rasmussen and Pedersen, 1979; Talwani et al., 1959) we derived the boundaries of the lower crust fitting the observed gravity (Figure A6). The difference between the top boundaries of the lower crust in the two cases is minimal (i.e., less than 3 km and in order of possible RF error) in Zagros but for Alborz it reaches to a maximum difference of 5 km. The difference between the bottom boundaries of the lower crust in the two cases are larger and could reach to a maximum value of 10 km for the Alborz root but for the Zagros root the difference is about 4 km. This test shows that the change in the boundaries is larger than the possible RF depth conversion errors especially in Alborz.

959

960

961

Table A1 : The sensitivity of the model to the density of the Caspian shallow anomaly

Number of test	1	2	3	4	5	6	7
Caspian shallow anomaly	2800	2850	2900	2950	3000	3050	3100

962 .

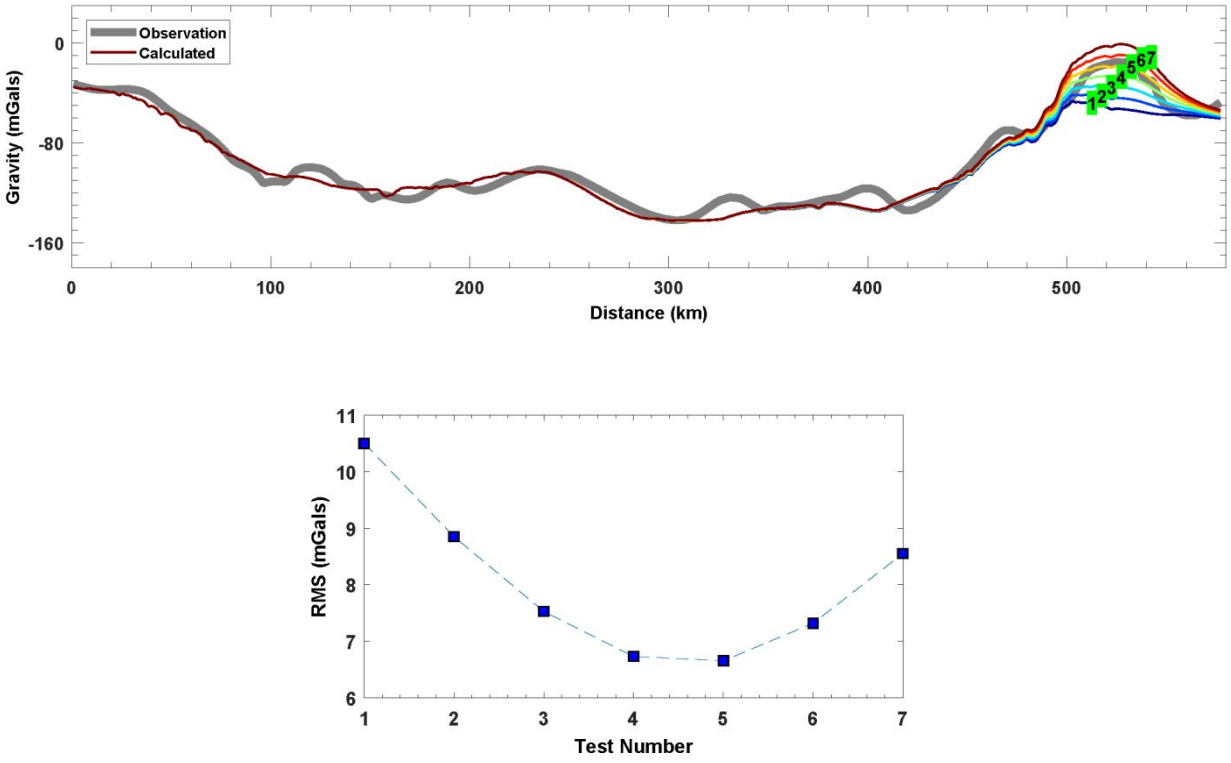

Figure A1: The sensitivity of the model to the density of the shallow high density Caspian body.The observed Bouguer anomaly (thick gray line) and calculated Bouguer anomalies

(thin colorful lines) for different crustal density of the shallow high density Caspian body (the top panel). The numbers on the top panel corresponds to the models listed in the Table A1. The bottom panel shows RMS misfit for different models. The RMS values are related to the difference between the calculated and observed gravity anomalies. The RMS misfit is minimum for density of 2950 to 3000 kg/m^3.

963 .

964

TableA2: The sensitivity of the density model to the density of the Alborz root

Number of test	1	2	3	4	5	6	7
Density (kg/m^3)	2950	3000	3050	3100	3150	3200	3250

965 .

966

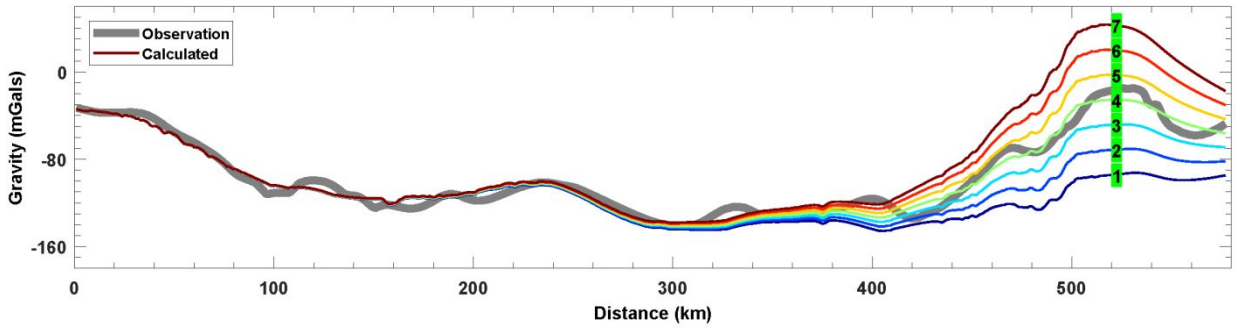

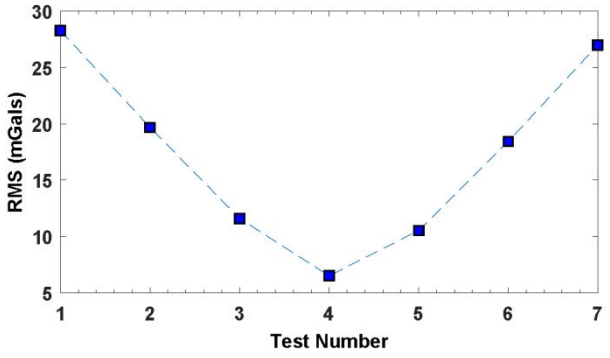

Figure A2: The sensitivity of the density model to the density of the Alborz root.The observed Bouguer anomaly (thick gray line) and calculated Bouguer anomalies (thin colorful lines) for different crustal density of Alborz crustal root (the top panel).The numbers on the top panelcorresponds to the models listed in the Table A2.The bottom panel shows RMS misfit for different model. The RMS values are related to the difference between the calculated and observed gravity anomalies. The RMS misfit is minimum for density of 3100 kg/m^3.

967 .

TableA3: The sensitivity of the model to variations of the density of the Zagros root

Number of test	1	2	3	4	5	6	7	8
Zagros root	2900	2950	3000	3050	3100	3150	3200	3250

968 .

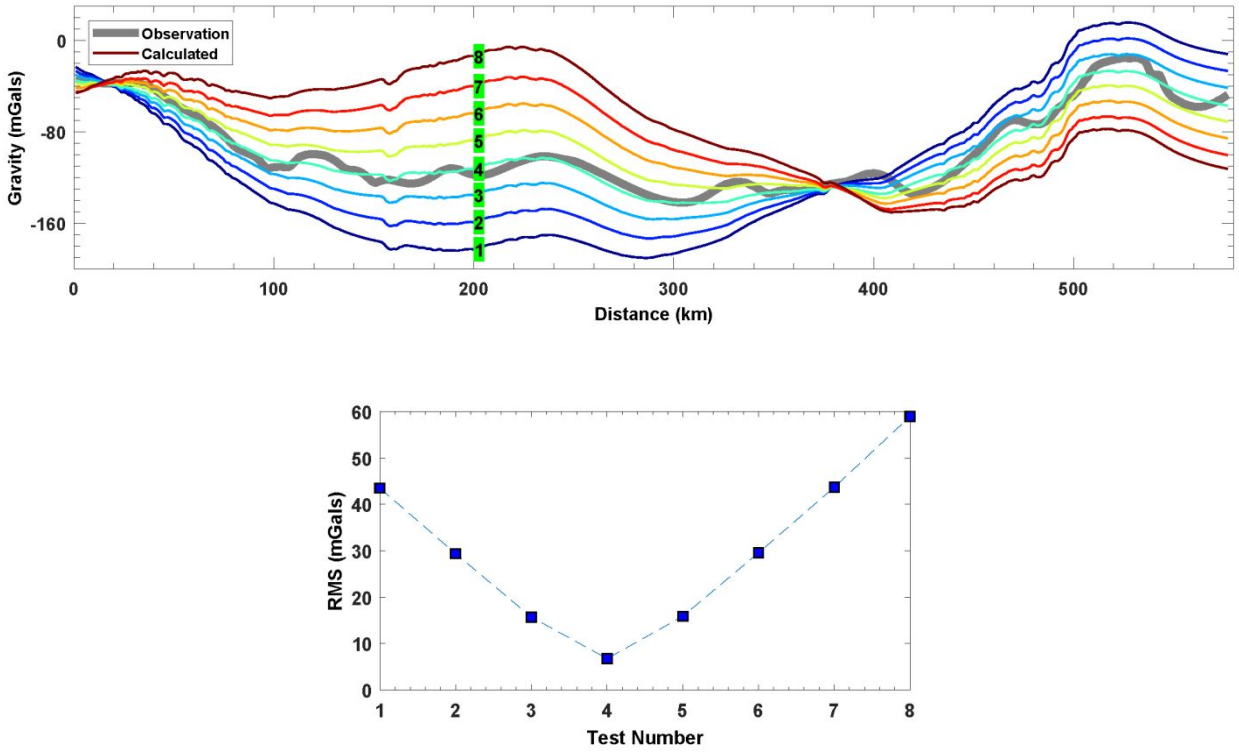

Figure A3: Top panel shows Bouguer anomaly for different density valuesfrom 2900 kg/m3 to 3250 kg/m3 for the Zagros root. Numbers indicate index number is same in the table A3 and horizontal axes of the Root Mean Square (RMS) misfit figure. The RMS valuesindicates that the calculated anomaly is sensitive to the density of Zagros's root and the density value of 3050 kg/m^{3}produces the best fit between observation and calculation.

969 ..

970

971

972

Table A4 :The sensitivity of the model to the different combination of density for Zagros root and Alborz root

Number of test	1	2	3	4	5	6	7	8	9
Zagros root	2950	3000	3050	3100	3150	3200	2950	3000	3050
Alborz root	2950	2950	2950	2950	2950	2950	3000	3000	3000
Number of test	10	11	12	13	14	15	16	17	18
Zagros root	3100	3150	3200	2950	3000	3050	3100	3150	3200
Alborz root	3000	3000	3000	3050	3050	3050	3050	3050	3050
Number of test	19	20	21	22	23	24	25	26	27
Zagros root	2950	3000	3050	3100	3150	3200	2950	3000	3050
Alborz root	3100	3100	3100	3100	3100	3100	3150	3150	3150
Number of test	28	29	30	31	32	33	34	35	36
Zagros root	3100	3150	3200	2950	3000	3050	3100	3150	3200
Alborz root	3150	3150	3150	3200	3200	3200	3200	3200	3200

973 .

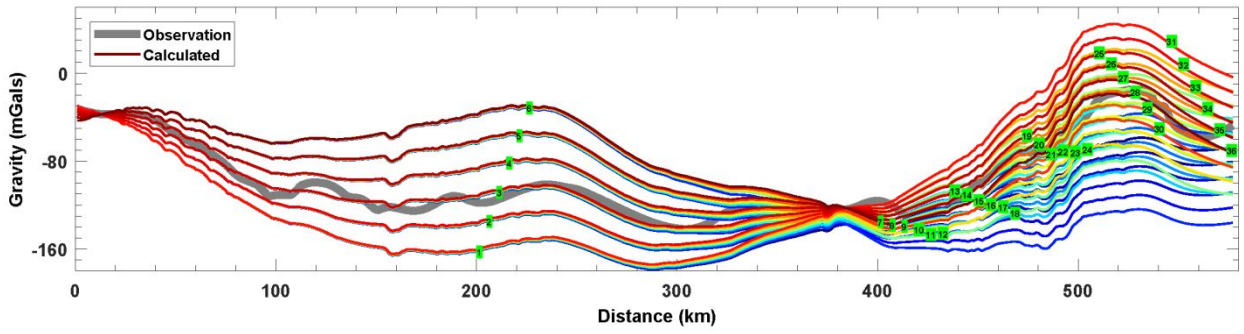

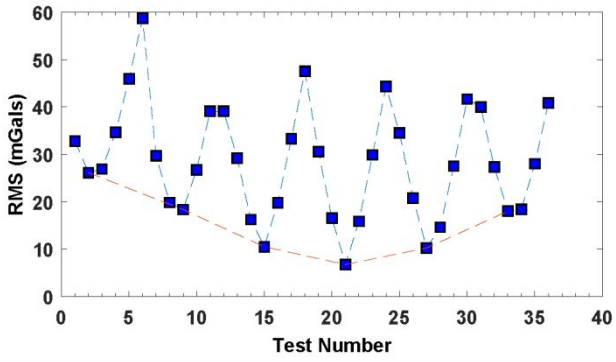

Figure A4: The sensitivity of the model to the different combinations of density for Zagros root and Alborz root (Table 4). In this test, different density value for the Alborz and Zagros roots is considered to find best fit solution for the different combinations. Results indicates that the response of the model dependsonthe density of the roots and the best solution occur for density of 3050 kg/m^3 for Zagros root and 3100 kg/m^3 for Alborz root.

974 .

975

Table A5: The sensitivity of the model to the different scenario of density of upper and lower crust.

Number of test	1	2	3	4	5	6	7	8	9
Upper crust	2650	2700	2750	2800	2800	2800	2800	2800	2800
Middle crust	2800	2800	2800	2850	2900	2900	2900	2900	2900
Lower crust	2900	2900	2900	2900	2950	3000	3000	3000	3000
Zagros root	3000	3000	3000	3000	3050	3100	3150	3200	3250
Alborz root	2950	2950	2950	2950	3000	3050	3050	3050	3050

Number of test	10	11	12	13	14	15	16	17	18
Upper crust	2800	2800	2800	2800	2800	2800	2800	2800	2800
Middle crust	2900	2900	2900	2900	2900	2900	2900	2900	2900
Lower crust	3000	3000	3000	3000	3000	3000	3000	3000	3000
Zagros root	3100	3150	3200	3250	3100	3150	3200	3250	3100
Alborz root	3100	3100	3100	3100	3150	3150	3150	3150	3200

976 .

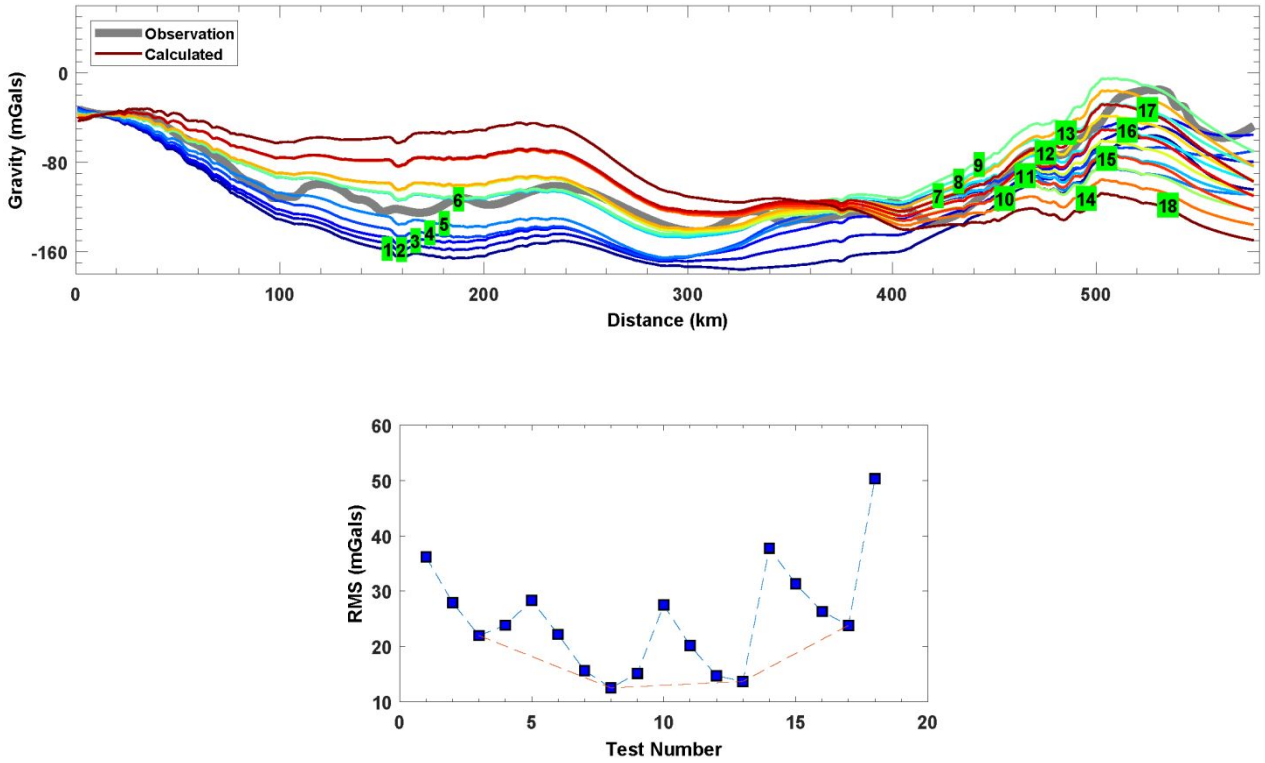

Figure A5: Sensitivity analysis of crystalline crust of the 2D density model where the properties of the upper, middle, and lower crust were altered according to scenarios given in Table A5. The numbers on the top panel corresponds to the models listed in the Table A5. The

bottom panel shows RMS misfit for different models. The RMS values are related to the difference between the calculated and observed gravity anomalies. The RMS misfit is minimum for scenario 8 (Table 5).

977 .

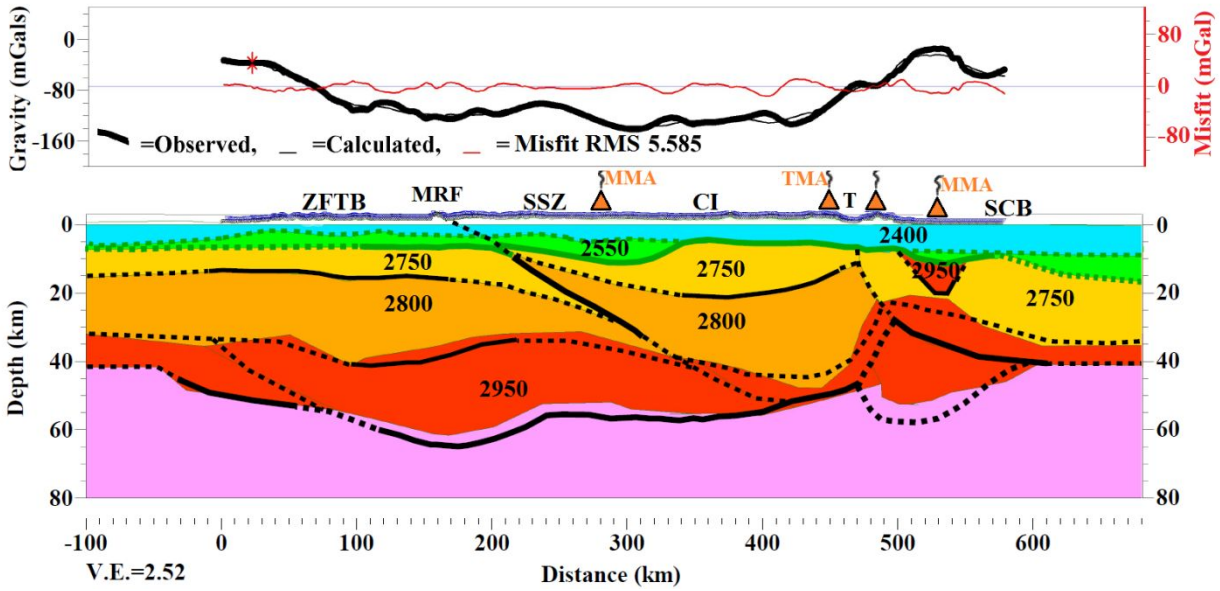

Figure A6: Sensitivity analysis of the model to the shape of lower crust while assuming a constant density of lower crust of 2950 kg/m^3 (i.e., no dense crustal root is considered) and assigning the density of all the shallower units to those used in Figure 6. The top and bottom boundaries of the lower crust are calculated using an inversion method. The new calculated boundaries of lower crust are shown by a red polygon. This new model provides a solution with an RMS misfit around 5.58 mGal, which should be compared to the RMS misfit for the final model of 6.64 mGal. All the crustal boundaries from Figure 6 are superimposed on the figure.

978 .

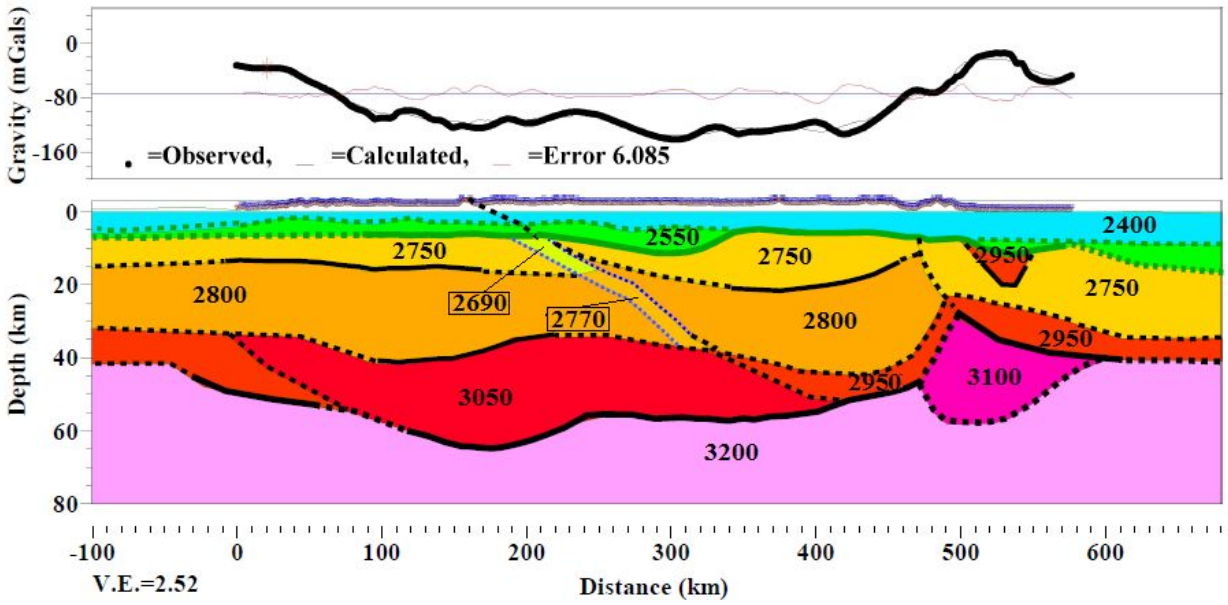

Figure A7: Density model of possible low velocity (and density) zone in a more straight way by introducing a low density area

979

980 **References :**

981 Artemieva, I.M., Thybo, H., 2013. EUNAseis: A seismic model for Moho and crustal structure in
982 Europe, Greenland, and the North Atlantic region. Tectonophysics 609, 97–153.
983 doi:10.1016/j.tecto.2013.08.004

984 Rasmussen, R., Pedersen, L.B., 1979. End corrections in potential field modeling. Geophys.
985 Prospect 27(4), 749–760.

986 Talwani, M., Worzel, J.L., Landisman, M., 1959. Rapid gravity computations for two-dimensional
987 bodies with application to the Mendocino submarine fracture zone. J. Geophys. Res. 64, 49–
988 59. doi:10.1029/JZ064i001p00049

989